Title

FBXL12 degrades FANCD2 to regulate replication recovery and promote cancer cell survival under conditions of replication stress

Journal

Molecular Cell, 83(20)

ISSN

1097-2765

Authors

Brunner, Andrä
Li, Qiuzhen
Fisicaro, Samuele
et al.

Publication Date

2023-10-01

DOI

10.1016/j.molcel.2023.07.026

Peer reviewed

HHS Public Access

Author manuscript

Mol Cell. Author manuscript; available in PMC 2024 October 19.

Published in final edited form as:

Mol Cell. 2023 October 19; 83(20): 3720–3739.e8. doi:10.1016/j.molcel.2023.07.026.

FBXL12 degrades FANCD2 to regulate replication recovery and promote cancer cell survival under conditions of replication stress

Andrä Brunner[1,*], **Qiuzhen Li**[1], **Samuele Fisicaro**[1], **Alexandros Kourtesakis**[1], **Johanna Viiliäinen**[1], **Henrik J. Johansson**[2], **Vijaya Pandey**[3], **Adarsh K. Mayank**[3], **Janne Lehtiö**[2], **James A. Wohlschlegel**[3], **Charles Spruck**[4], **Juha K. Rantala**[5,6], **Lukas M. Orre**[2], **Olle Sangfelt**[1,*,#]

[1]Department of Cell and Molecular Biology, Karolinska Institutet, Solna, 17165, Stockholms län, Sweden

[2]Department of Oncology and Pathology, Karolinska Institutet, Science for Life Laboratory, Solna, 17165, Stockholms län, Sweden

[3]Department of Biological Chemistry, University of California, Los Angeles, 90095, California, USA

[4]NCI-Designated Cancer Center, Sanford Burnham Prebys Medical Discovery Institute, La Jolla, 92037, California, USA

[5]Department of Oncology and Metabolism, University of Sheffield, Sheffield, S10 2RX, South Yorkshire, United Kingdom

[6]Misvik Biology, Turku, 20520, Finland

SUMMARY

Fanconi anaemia signalling, a key genomic maintenance pathway, is activated in response to replication stress. Here, we report that phosphorylation of the pivotal pathway protein FANCD2 by CHK1 triggers its FBXL12-dependent proteasomal degradation, facilitating FANCD2 clearance at stalled replication forks. This promotes efficient DNA replication under conditions of CYCLIN E- and drug-induced replication stress. Reconstituting FANCD2-deficient fibroblasts with phosphodegron mutants failed to re-establish fork progression. In the absence of FBXL12, FANCD2 becomes trapped on chromatin leading to replication stress and excessive DNA

[*]Corresponding authors: andra.brunner@ki.se and olle.sangfelt@ki.se.
[#]Lead contact

AUTHOR CONTRIBUTIONS

Conceptualisation, A.B. and O.S.; Methodology, A.B., J.A.W. and J.K.R.; Investigation, A.B., Q.L., S.F., A.K., J.V., H.J.J., V.P., A.K.M. J.K.R. and O.S.; Resources, J.L.; Writing- Original draft, A.B.; Writing – Review & Editing, A.B., C.S., L.M.O. and O.S.; Visualisation, A.B., J.K.R. and L.M.O.; Supervision, O.S.; Project administration, A.B. and O.S.; Funding acquisition, O.S.

DECLARATION OF INTERESTS

The authors declare no competing interests.

damage. In human cancers, FBXL12, CYCLIN E, and Fanconi anaemia signalling are positively correlated and FBXL12 upregulation is linked to reduced survival in patients with high CYCLIN E expressing breast tumours. Finally, depletion of FBXL12 exacerbated oncogene-induced replication stress and sensitised cancer cells to drug-induced replication stress by WEE1 inhibition. Collectively, our results indicate that FBXL12 constitutes a vulnerability and a potential therapeutic target in CYCLIN E-overexpressing cancers.

Graphical Abstract

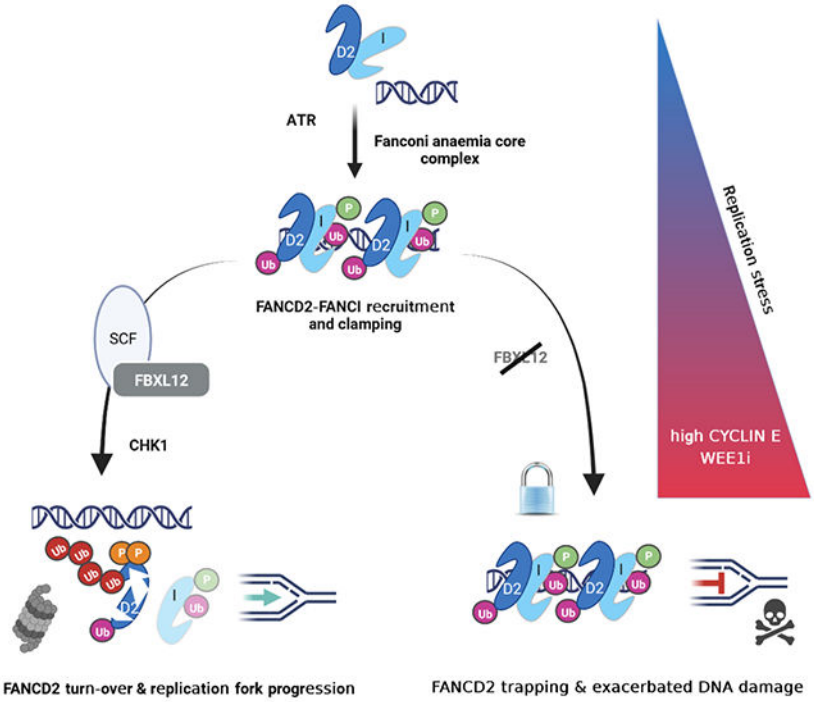

eTOC blurp

The Fanconi anaemia pathway alleviates oncogene-induced replication stress. Brunner et al. report that the ubiquitin ligase SCF^{FBXL12} targets the key Fanconi anaemia protein FANCD2 for proteasomal degradation. They demonstrate that this occurs in the vicinity of replication forks and is critical for replication recovery and survival under CDK-driven replication stress.

Keywords

FBXL12; replication stress; Fanconi anaemia; FANCD2; CYCLIN E; SCF ubiquitin ligase

INTRODUCTION

The occurrence of oncogene-induced replication stress (OIRS) is a common early event in the multistep process of cancer development[1]. Activation of oncogenes such as CYCLIN E or c-MYC leads to replication stress (RS), signified by reduced replication fork speed, through deregulation of cell cycle progression or transcription programs that result in fork

collapses and one-ended double-strand breaks (DSBs)[2–5]. Clinically, targeting oncoproteins has proven problematic, thus an alternative targeted approach is to focus on pathways that enable survival under OIRS[6].

In the context of OIRS, *CCNE1* is one of the most thoroughly studied oncogenes owing to its frequent overexpression and association with poor patient outcome[7–9]. Through its CDK2 activator function, overexpression of CYCLIN E has been demonstrated to shorten G1 phase, promote premature S-phase entry and reduce the number of licensed replication origins while increasing the proportion of firing origins, leading to increased conflicts between transcription and replication machineries[10]. CYCLIN E overexpression also causes fork slowing, fork reversal and nucleotide depletion, ultimately resulting in DNA breaks and DNA damage response (DDR) activation during G2/M and chromosomal instability[10–13]. CYCLIN E-induced RS results in activation of ATR and, downstream, CHK1 kinases which regulate a multitude of RS response pathways to limit DNA damage and restrict nucleolytic processing of unresolved replication intermediates to G2/M phase[13]. This notion is supported by synthetic lethal interactions between CYCLIN E overexpression and ATR or CHK1 inhibition, which is accompanied by massive DNA damage, threatening cancer cell survival[14]. However, despite their relevance for cancer treatment, pathways that counteract the deleterious effects of OIRS remain incompletely understood.

Fanconi anaemia (FA) signalling is one of the major pathways that maintain genomic integrity through recruitment and stabilisation of components of DDR pathways, such as the homologous recombination repair (HRR) proteins BRCA1/2[15–17]. While the classical function of the FA pathway is the repair of inter-strand crosslinks (ICLs), its crucial roles in counteracting RS have become increasingly apparent[18]. The key FA proteins, FANCD2 and FANCI, safeguard stalled replication forks[19] and facilitate new origin firing[20] . When replication forks stall, FANCD2-FANCI (ID2) dimers are recruited to chromatin, clamp around DNA and become monoubiquitinated[21–23]. Although ID2 clamp closure occurs independently of FANCD2 monoubiquitination, this modification stabilizes the clamped conformation[21–24]. The deubiquitinating enzyme USP1 in complex with UAF1 can remove monoubiquitin from FANCD2[25], presumably to promote the re-opening of the ID2 clamp. However, how the fully engaged di-mono-ubiquitinated complex (Ub-FANCD2-Ub-FANCI), which is no longer a substrate for USP1-UAF1[24], is removed, remains elusive. Nevertheless, this step is critical to complete the pathway once conditions are permissive for replication fork recovery. Here, we show that SCF-FBXL12 acts as an E3 ligase that polyubiquitinates and targets CHK1-phosphorylated FANCD2 for proteasomal degradation. This mechanism is crucial for replication recovery and cell survival in the context of CYCLIN E overexpression or WEE1 inhibition.

RESULTS

FBXL12 suppresses CYCLIN E-induced replication stress and facilitates replication recovery

To identify regulators of replication recovery, we performed an imaging-based single-cell small interfering RNA (siRNA) screen in HCC1569 cells with amplification of *CCNE1*, as outlined in Fig. 1A. siRNAs directed against the F-box protein FBXL12 interfered with

recovery of replication after release from a replication block induced by aphidicolin (APH) (relative increase of BrdU+/EdU− labelled cells) (Fig. 1B and Fig. S1A and B). Supporting the screening approach, siRNAs targeting FBXW7, the SCF substrate receptor mediating CYCLIN E degradation[26], also compromised replication recovery (Fig. 1B) and in line with the exacerbated sensitivity of CYCLIN E overexpressing cells to ATR inhibitors[8,14,27], ATR siRNAs attenuated incorporation of both nucleotide analogues (Fig. S1C and Table S1). Consistently, knockdown of FBXL12 enriched BLBC cells in the S-G2 phase (Fig. S1D–G), increasing the proportion of non-replicating (EdU-negative) cells (Fig. S1H).

Increased or decreased DNA replication can be attributed to an altered capacity to rescue stalled or damaged forks or changes in the activation of new origins. To distinguish these different parameters of replication recovery, we performed single-molecule DNA fibre analysis, analogous to the single-cell siRNA screen (Fig. 1C). Knockdown of FBXL12 in HCC1569 cells increased the proportion of stalled forks and the number of new origins firing (Fig. 1C). Consistent with the DNA fibre results, inhibition of new origin firing with CDC7 inhibitors (XL413) reduced replication recovery in FBXL12-depleted S-phase cells at the single cell level (Fig. 1D). To establish whether CYCLIN E overexpression is a prerequisite to reduced replication fork processivity in the absence of FBXL12, we performed DNA fibre assays following sequential pulse labelling of U2OS cells (in which doxycycline (dox)-regulated expression of CYCLIN E promotes DNA RS[3,28]) with CldU and IdU, and measured IdU track length. FBXL12 depletion only mildly affected replication fork progression in the absence of CYCLIN E overexpression (+dox), but it amplified the effect upon CYCLIN E overexpression (-dox), resulting in a significant decrease in the length of replication tracks (Fig. 1E, Fig. S1I and J). Additionally, we assessed fork recovery using APH as well as hydroxyurea (HU) to temporarily block replication forks, and again found that FBXL12 depletion reduced the proportion of restarted forks and decreased the track length of elongating forks, particularly upon CYCLIN E induction (Fig. S1K and L).

Proteomic profiling of a panel of 17 breast cancer cell lines showed that FBXL12 correlated positively with CYCLIN E1 expression (Fig. 1F), but not significantly with other oncogenes (Fig. S2A). Analysis of mRNA expression levels in cell lines using the DepMap portal[29] confirmed positive correlation between *FBXL12* and *CCNE1*, which was more pronounced in breast cancer-derived cells (Fig. S2B and C). Further, expression of FBXL12 increased in cells overexpressing CYCLIN E, either by doxycycline-induced expression in U2OS cells or through stabilisation by FBXW7 deletion in HCT116 cells (Fig. 1G and Fig. S2D and E), indicating that FBXL12 may be upregulated to alleviate CYCLIN E-induced RS.

As prolonged fork stalling and excessive origin firing can result in replication fork collapse and formation of DSBs[30,31], we assessed if FBXL12 attenuates RS-associated DNA damage by analysis of pan-nuclear H2AX phosphorylation (γH2AX). FBXL12 knockdown increased the proportion of pan-γH2AX-stained nuclei in cancer cell lines with high CYCLIN E expression (Fig. 1H), while knockdown only marginally increased pan-γH2AX staining in untransformed immortalised cells and luminal breast cancer cell lines with low levels of CYCLIN E (Fig. 1H). As expected, depletion of FBXL12 in U2OS cells overexpressing CYCLIN E increased phosphorylation of H2AX and DNA replication checkpoint kinase CHK1 (Fig. 1I). To directly assess if depletion of FBXL12 generates

DSBs, we conducted neutral comet assays in HCC1569 and MCF10A cells. FBXL12 knockdown resulted in increased DSB formation in HCC1569 cells, while MCF10A cells remained unaffected (Fig. 1J).

FBXL12 sustains genome stability and promotes unrestricted proliferation in BLBC cells

To investigate the long-term effects of FBXL12 inhibition in BLBC cells, we first attempted to knockout FBXL12 using CRISPR-Cas9 genome editing in HCC1569 cells but failed to obtain viable clones. Instead, we generated inducible FBXL12 shRNAs in HCC1569, MDA-MB-231, and MCF10A cell lines. Prolonged knockdown (10 day) of FBXL12 resulted in a near-complete loss of viability of HCC1569 cells (Fig. 2A, 2B and Fig. S3A) while MCF10A cells proliferated normally (Fig. 2C and Fig. S3A). Long-term knockdown of FBXL12 in MDA-MB-231 cells with moderate levels of CYCLIN E resulted in an intermediate phenotype in which the cells continued to proliferate, albeit at a reduced rate with an increased proportion of cells with >4N DNA content, indicative of re-replication (Fig. S3B and C). Consistent with MCF10A cells being unaffected by FBXL12 depletion, no apparent activation of DNA damage markers γH2AX or CHK1 phosphorylation was detected, while these markers were highly expressed in MDA-MB-231 and HCC1569 cells (Fig. S3D).

Next, we generated several MDA-MB-231 FBXL12-KO cell lines, which all exhibited reduced cell proliferation (Fig 2D) and slower S-phase progression based on EdU pulse-chase experiments (Fig. S3E). MDA-MB-231 FBXL12-KO cells increased the proportion of senescence-associated β-galactosidase (SA-β-gal)-positive cells and p21 expression, consistent with persistent DNA damage and induction of senescence under RS conditions (Fig. 2E and Fig. S3F). FBXL12-KO cells displayed irregularly shaped nuclei with an elevated number of micronuclei and polyploidization (Fig. 2F and Fig. S3G), indicating FBXL12 deficiency contributes to chromosomal instability, resembling CYCLIN E-induced RS in human cancer[32]. Under-replicated DNA can cause mitotic errors and genomic instability if not resolved through a mitotic DNA synthesis process known as MiDAS[33,34]. In the absence of MiDAS, ultra-fine anaphase DNA bridges (UFBs) are formed during chromosomal segregation in anaphase, predating the onset of broad chromosomal instability[35]. FBXL12 depletion increased UFBs (Fig. 2G), consistent with micronuclei formation and DNA replication defects (Fig. 2F and Fig. S3G).

FBXL12 interacts with Fanconi anaemia proteins FANCD2 and FANCI

To obtain mechanistic insight into FBXL12-dependent regulation of RS, we employed mass spectrometry to identify FBXL12 interacting proteins. In two independent experiments, we found several peptides corresponding to FA proteins FANCD2 and FANCI among the interactors, and as expected SCF complex components SKP1 and RBX1 (Fig. 3A, B and Table S2). Putative interacting proteins were significantly enriched for DNA replication and cell cycle-associated pathways, and for FA signalling proteins (Fig. S4A and B). Interaction of FBXL12 with FANCD2/FANCI was confirmed and validated by co-immunoprecipitation (co-IP) (Fig. 3C and 3D). Endogenous FBXL12 and FANCD2/FANCI interacted primarily in chromatin fractions and interactions were not disrupted by nuclease (benzonase) treatment, indicating that binding does not require DNA (Fig. 3D

and Fig. S4C). Depletion of FANCD2 or FANCI followed by FBXL12 IP showed that FANCI interaction was FANCD2-dependent (Fig. S4D). As shown in Fig. 3E, FANCD2 only co-immunoprecipitated with FBXL12, and not with other F-box proteins. supporting their specific interaction. To assess FBXL12's binding to FANCD2 as an SCF complex, we immunoprecipitated CUL1 in the presence of MLN4924, which inhibits neddylation and SCF ligase activation (stabilizing substrates). CUL1 co-purified FANCD2 in FBXL12-WT but not FBXL12-KO HEK293T cells (Suppl. fig 3E), confirming assembly of the SCF-FBXL12-FANCD2 complex. During unperturbed S-phase, and more so in response to increased RS and fork stalling, FANCD2 and FANCI form nuclear foci with other proteins involved in DNA repair[36]. To examine their spatial interaction, we scored colocalization of FANCD2 and FBXL12 in the presence or absence of MLN4924, with or without CYCLIN E overexpression. As shown in Fig. 3F, FANCD2 foci overlapped with FBXL12 in the presence of MLN4924, and the number of FANCD2-FBXL12 foci significantly increased in response to CYCLIN E overexpression, supporting their functional relation during CYCLIN E-induced RS (Fig. 3G and Fig. S4F).

FBXL12 targets chromatin-associated FANCD2 for degradation

To investigate if FBXL12 regulates the stability of FANCD2 through ubiquitin-mediated proteasomal degradation, we first performed *in vivo* ubiquitination experiments (see methods) and observed high-molecular smears corresponding to polyubiquitinated FANCD2 and FANCI (Fig. 4A). Notably, although both FANCD2 and FANCI were polyubiquitinated in FBXL12-WT cells, FBXL12-KO cells showed a significant reduction only of FANCD2-ubiquitin conjugates, suggesting FBXL12-mediated and specific FANCD2 polyubiquitination (Fig. 4A). Further, endogenous FANCD2 was polyubiquitinated in an FBXL12-dependent manner (Fig. 4B), and pulldown of polyubiquitinated proteins using Tandem Ubiquitin Binding Entities (TUBEs) verified ubiquitination of FANCD2 in cells (Fig. S5A). We next fractionated cells treated with proteasomal inhibitor MG132 and found enrichment of endogenous FANCD2 polyubiquitination smears in the chromatin fraction (Fig. S5B). As proteasomal inhibitors deplete the free pool of ubiquitin which can reduce monoubiquitination of chromatin-associated proteins[37], we performed additional experiments. As shown in Fig. S5C, MG-132 treatment decreased FANCD2 protein levels at chromatin, while the DNA crosslinking agent mitomycin C (MMC) which potently activates FA signalling[38,39] increased FANCD2 in the chromatin fraction, in particular monoubiquitinated FANCD2 (Fig. S5C). MMC treatment also increased FANCD2 polyubiquitination in an FBXL12-dependent manner (Fig. 4C), and purification of chromatin-associated endogenous FANCD2 confirmed polyubiquitination of FANCD2 in the presence of MG-132 (Fig. S5B), as well as other proteasomal inhibitors (Fig. S5D). To test if FANCD2 polyubiquitination by FBXL12 promotes its degradation, we co-transfected FANCD2 with increasing amounts of FBXL12. As shown in Figure 4D, FBXL12 reduced FANCD2 protein levels, and treatment with MG-132 rescued FANCD2 levels. Accordingly, expression of FBXL12-ΔF (an F-box-deleted mutant unable to interact with active SCF complexes) failed to reduce FANCD2 levels (Fig 4D and Fig. S5E). Further, expression of dNCUL1 (dominant negative CUL1 unable to bind SCF subunit RBX1 that recruits the SCF E2 conjugating enzyme) increased FANCD2 protein stability at chromatin, supporting SCF-mediated FANCD2 degradation (Fig. S5F). Conversely, doxycycline-induced overexpression

of FBXL12 in MDA-MB-231 cells reduced endogenous FANCD2 protein levels in the chromatin fraction even in the absence of exogenous DNA damage (Fig. S5G). Importantly, cycloheximide (CHX) chase experiments confirmed that degradation of both exogenous and endogenous chromatin-associated FANCD2 was prevented in FBXL12 depleted cells (Fig. 4E and 4F). Notably, FBXL12 depletion did not stabilise endogenous FANCD2 in the soluble fraction (Fig. 4F) but increased the pool of chromatin-associated FANCD2 after treatment with different replication fork-stalling drugs that activate the FA pathway (Fig. S5H). FBXL12 knockdown did not affect *FANCD2* mRNA expression confirming post-transcriptional downregulation of FANCD2 protein (Fig. S5I). The levels of a panel of other proteins associated with replication forks and present in the mass spectrometry screen for FBXL12 interactors were not appreciably altered in FBXL12-depleted cells (Fig. S5J).

In agreement with FBXL12 knockdown increasing DNA damage (Fig. 1H and 1J), γH2AX was not resolved efficiently following washout of MMC in FBXL12-depleted cells (Fig. 4F, *compare lane 5 and lane 10, 24h drug washout*). These results were recapitulated in FBXL12-depleted cells overexpressing CYCLIN E (Fig. 4G and Fig. S5K) and FBXL12-KO cells displayed an increased number of FANCD2 foci compared to FBXL12-WT cells treated with MMC (Fig. S6A). We also found that FBXL12-depleted cells treated with HU had increased numbers of FANCD2 and RAD51 foci, supporting recruitment of RAD51 on resected ssDNA strands by FANCD2-FANCI dimers[40] (Fig. 4H and Fig. S6B).

Altogether, these results demonstrate that the SCF(FBXL12) ubiquitin ligase targets chromatin-bound FANCD2 for proteasomal degradation and regulates replication fork recovery in response to CYCLIN E-induced RS (Fig. 4I).

Phosphorylation of the FANCD2 N-terminus by CHK1 promotes FANCD2 polyubiquitination by FBXL12

Next, we aimed to identify FANCD2 motifs essential for FBXL12 interaction and polyubiquitination. We generated a series of FANCD2 deletion mutants, narrowing down the putative interaction site to the N-terminal region encompassing amino acids (aa) 1–120 (Fig. S7A and 5B). As F-box proteins commonly interact with phosphorylated substrates[41], we examined the FANCD2 N-terminus for potential phosphorylation sites. The N-terminus of FANCD2 harbours consensus motifs for DNA repair and checkpoint kinases ATR, DNA-PK and CHK1. Interestingly, phosphorylation of serine 8 and serine 10 in FANCD2 (Fig. S7A) were reported in publicly available mass spectrometry screens[42]. Furthermore, these sites are evolutionarily conserved and match two nested CHK1 consensus motifs, RXXS and RXXXS/T, respectively (Fig. S7C). To test if FANCD2 phosphorylation by checkpoint kinases promoted its recognition and ubiquitination by FBXL12, we treated HEK293 cells with ATR (AZD6738), CHK1/CHK2 (AZD7762) or DNAPK (NU7441) inhibitors, respectively. ATR and CHK1 inhibition abrogated the interaction with FBXL12, indicating that phosphorylation of FANCD2 by ATR-CHK1 kinases regulate binding to FBXL12 (Fig. S7D). Next, we generated single amino acid substitution mutants of several serine residues in the FANCD2 N-terminus (amino acids 1–140), as well as a double alanine mutant of the putative CHK1 phosphorylation site (FANCD2-S8/10A, hereafter referred to as FANCD2-AA. FANCD2 and FBXL12 co-IPs showed that several FANCD2 mutants,

including S8A, S10A, S64A and S88A exhibited decreased FBXL12 interaction, albeit less profoundly compared to the FANCD2-AA double mutant which significantly reduced but did not fully abrogate FBXL12 interaction (Fig. 5A). Upon activation of the FA pathway with MMC, the full-length FANCD2-AA mutant also showed diminished interaction with FBXL12 (Fig. 5B).

To investigate if CHK1 phosphorylates the FANCD2 N-terminus, we translated the FANCD2 N-terminus and performed *in vitro* kinase assays. CHK1 phosphorylated FANCD2 as shown by immunoblotting with an antibody detecting phosphorylated serine or threonine within the RXXS/T motif (Fig. 5C). *In vitro* binding to peptides (encompassing the first 15 amino acids of FANCD2) which was phosphorylated by CHK1, confirmed that FBXL12 binds this phospho-motif (Fig. 5D), while two other F-box proteins with similar structure, SKP2 and FBXL5, failed to bind. Importantly, FBXL12 did not bind FANCD2 peptides with alanine mutations of the S8/S10 residues (Fig. 5D).

To provide additional evidence that SCF^{FBXL12} catalyses FANCD2 polyubiquitination and to assess the dependency on residues S8 and S10, we performed *in vitro* ubiquitination assays. As shown in Fig. 5E, full-length (FL) FBXL12, but not FBXL12-ΔF catalysed FANCD2 polyubiquitination. Correspondingly, FANCD2-AA was not polyubiquitinated by FBXL12 *in vitro* (Fig. 5E), or in cells (Fig. S7E), indicating that phosphorylation of FANCD2 at S8/S10 by CHK1 is required for efficient FANCD2 polyubiquitination. To examine if FANCD2 phosphorylation by CHK1 regulates FANCD2 protein levels, we co-expressed FANCD2 and FANCI in FBXL12-WT and FBXL12-KO HEK293T cells. As shown in Fig. 5F, CHK1 inhibition increased FANCD2 protein in chromatin fractions of FBXL12-WT cells, to levels comparable to FBXL12-KO cells (Fig. 5F, *compare lanes 2, 3 and 4*). Comparably, FANCD2-S8A and S10A levels were not significantly different in FBXL12-WT and FBXL12-KO cells (Fig. 5F*, lanes 6 – 9*), supporting FANCD2 degradation by FBXL12 upon S8/S10 phosphorylation by CHK1.

We next searched the ProteomicsDB peptide database[43] and found several N-terminal FANCD2 peptides previously reported to be modified with ubiquitin, including lysines 13 and 22. Typically, ubiquitination sites tend to be located within unstructured regions approximately 20 amino acids adjacent to the degron motif[44]. Based on this information, we created a K13R/K22R FANCD2 mutant (2KR mutant) along with a mutant containing five additional lysine mutations (from K13 to K34, 7KR mutant) and assessed polyubiquitination *in vitro*. Both the FANCD2 mutants had significantly reduced polyubiquitination smears as compared to WT-FANCD2 (Fig. 5G), indicating that lysines 13/22 are likely conjugated to ubiquitin by SCF^{FBXL12}, promoting FANCD2 degradation.

To investigate if K561-monoubiquitination influences FANCD2 phosphorylation and/or polyubiquitination by FBXL12, we performed MS-based proteomics using HEK293 cells co-transfected with monoubiquitin-deficient K561R-FANCD2 and FANCI, or CHK1 phosphorylation-deficient FANCD2-AA mutant as control. To induce rapid activation of CHK1, we inhibited WEE1 kinase using AZD1775[45]. The MS results did not reveal any conclusive FANCD2 ubiquitin-conjugated peptides, however, we identified several phosphorylated N-terminal peptides in the K561R-FANCD2 sample, including S8, S10

and S15 (Fig. 5H and Table S3), demonstrating that K561R is phosphorylated in response to RS induced by AZD1775. To test if monoubiquitination of FANCD2 influences FBXL12-mediated FANCD2 polyubiquitination, we depleted FANCL, and for comparison USP1 (which removes K561-monoubiquitin) and performed *in vivo* ubiquitination assays. Depletion of FANCL (or USP1) did not prevent FBXL12-dependent FANCD2 polyubiquitination (Fig. S7F), and as expected, expression of FBXL12 downregulated K561R-FANCD2 in a dose-dependent manner, like WT-FANCD2 (Fig. 5I). Additional analysis with the K561R mutant corroborated polyubiquitination in the absence of K561 monoubiquitination (Fig. S7G) and both WT-FANCD2 and K561R-FANCD2 were increased in FBXL12-KO cells, supporting FANCD2 degradation independent of its monoubiquitination state (Fig. S7H).

FBXL12 alleviates CYCLIN E-induced and CDK-driven replication stress in a FANCD2-dependent manner

To discern the physiological role of FBXL12-mediated degradation of FANCD2, we assessed replication fork progression and origin usage in *CCNE1* amplified HCC1569 cells following depletion of either FBXL12, FANCD2, or their co-depletion. While knockdown of FBXL12 or FANCD2 individually decreased replication fork speed, their co-depletion restored fork progression to the same level as control cells (Fig. 6A). Similarly, the proportion of stalled replication forks increased with FANCD2 or FBXL12 silencing, though co-silencing of FANCD2/FBXL12 re-established the number of stalled replication forks analogous to control (Fig. 6B). These effects are likely due to residual expression of FANCD2 following siRNA-mediated downregulation, whereby the combined FBXL12-FANCD2 knockdown results in functionally sufficient FANCD2 levels to support fork recovery and fork progression (Fig. 6B and C). Interestingly, however, firing of new origins was specifically increased in FBXL12-depleted but not in FANCD2-depleted HCC1569 cells (Fig. 6B). Again, the combined depletion of FBXL12 and FANCD2 resulted in a significantly lower proportion of cells with new origin firing compared to control cells (Fig. 6B). Together, the data indicate an epistatic function of FBXL12 and FANCD2, as (partial) knockdown of FANCD2 alleviates the RS phenotypes that derive from depletion of FBXL12. Importantly, γH2AX immunoblotting revealed that the rescued replication fork processivity in FBXL12/FANCD2 co-depleted cells (Fig. 6B) reverted the increased DNA damage resulting from individual depletion of FBXL12 or FANCD2 (Fig. 6C). In line with these findings, the FANCD2-AA mutant was less efficient than WT-FANCD2 in reducing CYCLIN E-induced RS and ensuing DNA damage, as expression of FANCD2-AA increased γH2AX and p21 in response to CYCLIN E overexpression, compared to FANCD2-WT or control transfected cells (Fig. S8A). FBXL12 depletion also increased the percentage of 53BP1 nuclear bodies (NBs) in response to overexpression of CYCLIN E (Fig. 6D) and co-depletion of FANCD2 and FBXL12 rescued the formation of 53BP1 NBs in damaged daughter cells[47] (Fig. 6D), presumably reflecting that defective turnover of FANCD2 during chromosomal segregation in anaphase results in unresolved UFBs (Fig. S8B).

As a different approach to induce CDK1/2-driven RS (and activation of ATR-CHK1 signalling[48]) in addition to CYCLIN E, we conducted additional experiments using AZD1775. Similar to CYCLIN E overexpression, WEE1 inhibition leads to increased

origin firing, slower replication fork speeds, pre-mature mitosis and genomic instability[10,49]. Initially, AZD1775 treatment increased FANCD2 protein levels at chromatin. However, upon washout of AZD1775, the amount of FANCD2 decreased in a manner dependent on FBXL12 (Fig. S8C), reminiscent of FA pathway activation by MMC treatment and CYCLIN E-induced RS (Fig. 4E–G).

To directly assess if FBXL12 and FANCD2 bind to nascent DNA in the vicinity of replication forks, we performed aniPOND experiments as described[50]. Both FBXL12 and FANCD2 associated with replication forks in MDA-MB-231 cells (Fig. 6E and Fig. S8D) and upon AZD1775 treatment, FANCD2 was depleted in FBXL12-WT cells, in sharp contrast to FBXL12-KO cells where FANCD2 protein levels was significantly enriched (Fig. 6E). While thymidine-chase displaced replication fork protein PCNA, FANCD2 was captured on DNA after the replication fork passed, supporting spatial targeted degradation of FANCD2 at the replication fork (Fig. 6E). Analysis of KAP1 and γH2AX phosphorylation revealed a spike of DNA damage signalling in the vicinity of replication forks, which persisted in FBXL12-KO cells after the replication fork had passed (Fig. 6E), in agreement with unresolved DNA damage in FBXL12-depleted cells (Fig. 1).

As phosphorylation of the FANCD2 N-terminus by CHK1 regulates FBXL12-mediated polyubiquitination (Fig. 5), we hypothesized that mutation of S10 may interfere with fork progression during RS in a FANCD2-dependent manner. The Passmore lab recently showed that the disordered FANCD2 N-terminus undergoes a conformational change upon ATR-mediated phosphorylation of a flexible phospho-loop in FANCI, stimulating the transition of the ID2 complex from an open (unstable) to closed (stable) state[51]. Closure of the FANCD2-FANCI heterodimer then primes the ID2 complex for monoubiquitination and DNA clamping[21]. Notably, germline mutations in FANCD2 at position 10 (S10P) have been reported (Fanconi anemia mutation database - https://www2.rockefeller.edu/fanconi/). To the best of our knowledge, the significance of S10P mutation in FA patients is unknown. To investigate the functional effects of mutating the FANCD2 phosphodegron, we used FANCD2-deficient FA patient fibroblasts (PD20) as a model[52] and reconstituted FANCD2-WT, -AA and -S10P, and additionally S10D, as a phosphomimetic mutant in PD20 cells (Fig. 6F). The constructs were expressed at low levels to avoid artefacts related to overexpression and all mutants interacted with FANCI (Fig. S8E). Notably, we found that the recruitment of FANCI to chromatin in PD20 (and HCC1569) cells depends on FANCD2 (Fig. 6C and Fig. S8G). As expected, the FANCD2-S10D mutant was consistently detected at lower levels (Fig. S8F) and its turnover rate on chromatin was comparable to FANCD2-WT, while the FANCD2-S10P and -AA mutants were stable (Fig. 6G).

Importantly, PD20 cells reconstituted with either FANCD2-AA or FANCD2-S10P failed to promote cell survival in response to AZD1775 treatment, and to a lesser extent, MMC-treatment, in contrast to PD20 cells expressing FANCD2-WT (Fig. 6H, 6I and Fig. S8H). Consistent with a protective role of FANCD2 during RS, AZD1775 treatment significantly increased DSB formation in PD20 cells compared to PD20 FANCD2-WT cells (Fig. 6J). Importantly, PD20 cells reconstituted with the FANCD2 AA or S10P mutant were unable to prevent DNA damage induced by AZD1775 (Fig. 6I and 6J). Finally, to provide direct functional evidence of the FANCD2 N-terminal degron in regulating replication fork

progression we performed additional DNA fibre assays. Strikingly, both AA and S10P mutants significantly reduced fork progression as compared to WT-FANCD2 (Fig. 6K). Thus, PD20 cells reconstituted with polyubiquitination-deficient FANCD2 mutants have reduced RF processivity in response to CDK-driven RS and mutation of S10 disrupted the protective function of FANCD2. Deletion of FBXL12 in PD20 cells (PD20-FBXL12-KO) did not change the rate of proliferation as compared to parental PD20 cells, nor did it exacerbate DNA damage formation upon RS, further supporting FANCD2 dependency of the observed FBXL12 phenotypes (Fig. S8I–K). Consistently, siRNA depletion of FBXL12 significantly increased DNA damage in PD20-FANCD2-WT cells treated with AZD1775, as compared to PD20 cells (Fig. S8L).

The FBXL12-FANCD2 axis is overexpressed in highly proliferative tumours and its disruption causes sensitisation to drug-induced replication stress

We next interrogated public cancer transcriptomic data and found increased expression of *FBXL12* in basal-like and luminal A breast tumours (Fig. S9A) and strong positive correlation between *FBXL12* and *CCNE1, CHEK1* and *FANCD2*, particularly in breast cancer (Fig. S9B–E). In agreement with the function of FBXL12 and FANCD2 in mitigating OIRS, *FBXL12* expression correlated with *CCNE1* and several FA genes in the TCGA PanCancer dataset (Fig. 7A and Fig. S9F). *FANCD2* expression correlated strongly with *MKI67* expression, supporting its requirement in highly proliferative cells (Fig. S9G). Correlations between FBXL12, FANCD2 and CYCLIN E were more evident in the proteome cohorts of 45 breast[53] and 141 non-small cell lung cancers (NSCLC)[54]. In breast cancer, both FBXL12 and FANCD2 were significantly elevated in the BLBC subtype when stratified according to their PAM50 signature, which also coincided with high CYCLIN E2, MYC and MKI67 expression (CYCLIN E1 was absent in the proteome dataset) (Fig. 7B–D, Fig. S9H and I). Rank-based gene set enrichment analysis (GSEA) using this dataset with FBXL12 protein expression as a continuous variable demonstrated that genes correlating with FBXL12 were significantly enriched for E2F targets, G2/M checkpoint, DNA damage response, MYC targets, and interestingly interferon gamma/alpha response, characteristic features of genomically unstable BLBCs (Fig. S9J–M). Among the proteins that most strongly correlated with FBXL12 expression in the breast cancer dataset were USP1 and PARP2 (Spearman's correlation coefficients r=0.57 and r=0.62, respectively), which are intricately linked to HR/FA DNA damage response pathways (Fig. S9N). GSEA of FBXL12 protein correlations in the panel of breast cancer cell lines (Fig. 1) consistently revealed enrichment of E2F targets, as well as epithelial-to-mesenchymal transition and G2/M checkpoint (FDR<0.00025 for all three gene sets) (Fig. S9O). In lung cancer, increased expression of the FBXL12-FANCD2 axis was observed in subtype 5, which is distinguished by high proliferation, worse patient outcome and frequent overexpression of oncogenes[54] (Fig. S10A–F).

High *FBXL12* expression correlated with significantly decreased patient survival in lung and gastric cancer (Fig. S10G and H), while in breast cancer, increased expression was linked to improved survival (Fig. S10I). In contrast, when analysis was restricted to high-grade, chemotherapy-treated breast cancers, high *FBXL12* expression showed a trend towards poor patient outcome (Fig. S10J). To further assess the clinical significance and correlation

between FBXL12, CCNE1, and overall survival, we analysed TCGA breast cancer survival data[55] using a median *FBXL12* expression cut-off. Tumour samples stratified based on high or low *FBXL12* expression were then analysed in relation to *CCNE1* gene expression. Importantly, in the *FBXL12* high group, *CCNE1* high patients showed significantly lower survival compared to patients with low *CCNE1* expression (Fig. 7E, p=5.8e-3), while there was no significant difference between *CCNE1* high and low patients in the *FBXL12* low group (Fig. 7F, p=0.158). Moreover, a notable co-occurrence of *CCNE1* and *FBXL12* amplifications was observed in breast cancer patients ($p<0.0001$) and median progression-free survival was markedly reduced in patients with amplifications of both genes (Fig. 7G and Fig. S10K).

To determine if loss of FBXL12 causes deregulation of RS and DNA damage response pathways, we profiled the transcriptomes of two MDA-MB-231 KO clones and WT cells (Fig. 7H and Table S4). FBXL12-KO cells displayed significant upregulation of pathways linked to induction of senescence and cell death, and downregulation of several DNA damage and repair pathways, including HR/FA (Fig. S10L). We next created an FBXL12 gene signature comprising genes significantly upregulated at least 2.8-fold in FBXL12-KO cells to evaluate if FBXL12 is linked to deregulation of the RS response. The FBXL12-KO gene signature correlated with a published RS signature from MCF10A cells overexpressing CYCLIN E and depleted of central RS/DDR response regulators[56], applied on various gene expression datasets from TCGA cancer patient cohorts (Fig. 7I–L).

As CYCLIN E overexpression induces ssDNA gaps[57], a marker of RS, and HR-deficient cancer cells can accumulate ssDNA gaps at stalled replication forks[58], we scored ssDNA intensity in nuclei with nascent DNA (see methods). Since PARP inhibition interferes with repair of ssDNA breaks, we also treated cells with the PARP inhibitor Olaparib and found that in FBXL12-KO but not -WT cells Olaparib treatment resulted in significantly increased ssDNA intensity (Fig. 7M and Fig. S10M), supporting accumulation of ssDNA gaps and DNA damage upon depletion of FBXL12 in BLBC cells. Although TNBC cells are commonly HR defective (with mutations in BRCA1/2) only a fraction responds to PARP inhibitors. We performed comet and viability assays of Olaparib treated FBXL12-WT and KO cells and found that FBXL12 depletion sensitised TNBC MDA-MB-231 cells to PARP inhibitors (Fig. S10N and O).

Finally, to test whether FBXL12 depletion sensitised cancer cells to drug-induced RS, we treated MDA-MB-231 cells (FBXL12-WT and FBXL12-KO) with AZD1775 and assessed acute sensitivity and re-proliferation capacity. Although MDA-MB-231 cells respond to acute inhibition of WEE1 by AZD1775, they recover post-treatment[45]. Importantly, knockout of FBXL12 exacerbated sensitivity to low nanomolar AZD1775 concentrations (Fig. 7N) and impaired cellular recovery compared to FBXL12-WT cells (Fig. 7O). Consistently, FANCD2 protein was enriched at chromatin post AZD1775 treatment in FBXL12-depleted cells (Fig. 7P) which was also associated with a significant delay in clearance of γH2AX (Fig. 7Q), accordant with a dependency on FBXL12 in response to RS, comparable to CYCLIN E overexpressing cells (Fig. 1). Collectively, these data indicate that FBXL12 expression may be a useful indicator of patient outcome and a potential vulnerability in tumors with CYCLIN E overexpression.

DISCUSSION

In this study we show that FBXL12-mediated polyubiquitination and proteasomal degradation of FANCD2 at stalled replication forks promotes fork recovery and DNA synthesis in the context of CYCLIN E- and drug-induced RS (Fig. S11). To activate FA signalling, ATR-phosphorylates FANCI, enabling monoubiquitination of both FANCI and FANCD2 by the FA core complex[20]. This modification triggers a structural change, resulting in the formation of a stable clamped ID2 complex encircling the DNA[21,23]. De-ubiquitination of the monoubiquitinated ID2 complex by USP1-UAF1 stimulates its unloading from chromatin and knockdown of USP1 impairs subsequent DNA repair steps[59]. It is presently unclear how USP1 catalyses de-ubiquitination of the ID2 complex as monoubiquitinated FANCI occludes the USP1 interaction site in FANCD2[60]. Additionally, extraction of DNA bound ID2 complex may be initiated through sumoylation-ubiquitination involving the DVC1-p97 segregase complex, limiting ID2 dosage on chromatin[61].

Failure to remove the ID2 complex may lead to replication barriers that exacerbate DNA damage during replication stress, ultimately causing genome instability. Our findings shed light on the rapid removal of the ID2 complex, even in its di-monoubiquitinated (USP1-resistant) state, preventing potential replication obstacles. FBXL12 depletion and FANCD2 accumulation on chromatin not only reduced replication fork processivity and increased the proportion of stalled replication forks but also led to increased origin firing, seemingly contradictory to a report indicating an inhibitory effect of FANCD2 on dormant origin firing[20]. This could be explained by several observations: Firstly, stabilisation of FANCD2 also results in elevated levels of FANCI, possibly by formation of stable FANCD2-FANCI heterodimers[62]. Secondly, FANCI was attributed an activating role in dormant origin firing under mild RS conditions, however, phosphorylated FANCI is likely excluded from dormant origins as high RS resulted in sustained ATR-CHK1 activation and reduced dormant origin firing in the cited study[20]. Thirdly, we observed decreased amounts of FANCI present at chromatin in FANCD2-negative PD20 cells and following knockdown of FANCD2 in cancer cells. Thus, the likelihood of new origin firing is expected to vary based on the specific cell context and differ depending on the intensity and timing of RS.

Although both CHK1 and FANCD2 are general effectors of ATR signaling and DNA replication stress, ATR and CHK1 also have distinct functions. For instance, CHK1 inhibition leads to phosphorylation of ATR targets causing increased replication initiation and DNA strand breaks[63]. In addition, cancer synthetic lethality between ATR and CHK1 has been linked to increased CDK-dependent origin firing[64]. Our data show that CHK1 facilitates polyubiquitination of FANCD2 by FBXL12, presumably targeting of a pool of FANCD2 on chromatin that needs to be removed to allow replication recovery once conditions are favorable. Interestingly, slower fork progression in CHK1-inhibited cells is not caused by the excessive firing of new origins but was shown to result from the accumulation of replication barriers that compromise cell proliferation[65]. Evidently, spatiotemporal differences in CHK1 activity, early versus late replication origins and origin density will influence the local concentration of CHK1 at a particular fork/origin, further finetuning replication recovery with cell cycle progression. High expression of FANCD2 does not *per se* result in deregulation of fork dynamics, rather our data suggest that it is the

decreased FANCD2 protein turnover at replication forks that delays recovery. Analogously to other DNA repair factors recruited and trapped on DNA, such as PARP1 in the presence of PARP1 inhibitors, we suggest that defective turnover of FANCD2 results in a more severe functional impairment than complete FANCD2 loss under conditions of high RS, which may be due to increased difficulty in resorting to alternative pathways[66]. Elevated levels of FBXL12 and FANCD2 were observed in aggressive malignancies, particularly susceptible to high replication stress, and linked to unfavourable patient outcomes. This suggests that activation of the FBXL12-FANCD2 pathway may potentially contribute to development of drug resistance and that[67,68]FBXL12 could represent a potential cancer target, specifically in cancers exhibiting CYCLIN E overexpression and/or deregulation of CYCLIN E-CDK2 activity, for instance in tumours with *CCNE1* amplification or inactivation of the tumour suppressor gene *FBXW7*[69]. Intriguingly, CYCLIN E overexpression was shown to sensitise BLBCs to WEE1 inhibitor AZD1775 and PARP inhibition[70,71], and we demonstrate here that depletion of FBXL12 further sensitises cancer cells with moderate levels of CYCLIN E. Additionally, CHK1 inhibition induces RS and synthetic lethality in CYCLIN E overexpressing cells, as well as in MYC-driven lymphomas[14,72], indicating that the FBXL12-CHK1-FANCD2 axis might constitute a more general pathway for therapeutic intervention in cancers with high RS.

In summary, our study demonstrates that FBXL12 is a crucial suppressor of DNA replication stress through its function as an SCF substrate receptor for FANCD2. This pathway is vital for the survival of cancer cells under conditions of high RS, findings that may have important medical implications.

Limitations of the study

Our work primarily focused on FBXL12-mediated degradation of FANCD2 in the context of CDK-driven replication stress. The broader implications of this mechanism in cancer types and different sources of replication stress require further exploration. While the study provides evidence of a positive correlation between FBXL12, CYCLIN E, and Fanconi anaemia signalling, further investigation is needed to establish the potential efficacy and safety of targeting FBXL12-FANCD2 signalling as a therapeutic approach. It is also important to consider that FBXL12 may have regulatory effects on other proteins involved in different cellular processes.

STAR★Methods

References from key resource table:[10,20,32,45,52,73–81]

RESOURCE AVAILABILITY

Lead contact—Further information and requests for resources and reagents should be directed to and will be fulfilled by Olle Sangfelt (olle.sangfelt@ki.se).

Materials availability—All unique/stable reagents generated in this study are available from the lead contact without restriction.

Data and code availability

- All original data are available on GEO, MassIVE, Mendeley data and ProteomeXchange, respectively. All data are publicly available as of the date of publication. Accession numbers and DOI are listed in the key resources table.
- This paper does not report any original code.
- Any additional information required to reanalyse the data reported in this paper is available from the lead contact upon request.

EXPERIMENTAL MODEL AND STUDY PARTICIPANT DETAILS

Mammalian cell culture—HEK293, HEK293T, RPE-1 and U2OS cell lines were grown in Dulbecco's modified Eagle's medium (DMEM) supplemented with 10% FBS and 2mM L-glutamine. Medium for culturing U2OS CYCLIN E1 tet-off cells was furthermore supplemented with 1μg/ml puromycin and 1μg/ml doxycycline. HCC1569, SUM149PT, MDA-MB-231, CAL51, HCC1143, HCC1419, MCF7 and MDA-MB-157 breast cancer cell lines were grown in RPMI-1640 supplemented with 10% FBS and 2mM L-glutamine. MCF10A cells were maintained in DMEM supplemented with 10% FBS, 2mM L-glutamine and mammary epithelial growth supplement. PD20 fibroblasts were cultured in alpha-MEM supplemented with 15% FBS. All cells were incubated at 37°C in 5% CO2. Cell cultures were authenticated by short tandem repeat (STR) analysis. All cell lines were mycoplasma-free and periodically monitored using a PCR-based detection kit.

METHOD DETAILS

Antibodies and biochemical analysis—Whole cell lysates were obtained by lying cells in NP-40 lysis buffer (50 mM Tris-HCl [pH 8.0], 150 mM NaCl, 1% NP-40) supplemented with both protease (Complete mini) and phosphatase (PhosSTOP) inhibitors. In the case of immunoprecipitation experiments, lysates were incubated with respective antibodies for 16h, then incubated with Dynabeads coupled to protein G for 1h followed by three washes with lysis buffer. Subsequently, proteins were resolved by SDS-PAGE on 4–12% bis-acrylamide gels, blotted onto PVDF membranes, and detected by immunoblotting using the antibodies specified in the key resources table. For subsequent detection by chemiluminescence isotype-specific secondary antibodies coupled to horseradish peroxidase were used. Quantifications of immunoblot bands were obtained by densitometry analysis using ImageJ. Where plotted, data represent mean ± SEM based on at least three experiments.

Gene silencing and transfections—HEK293 and HEK293T cells were transfected by calcium-phosphate method as described elsewhere[82]. All other cell lines were transfected using TransIT LT-1 transfection reagent according to the manufacturer's information. For transient gene silencing siRNAs were transfected using HiPerfect according to the manufacturer's instructions. Cells were transfected 48 to 72h prior to analysis or functional assays.

CRISPR genome editing—Cas9 and guide RNAs were either transiently introduced by transfection described above (HEK293T) or stably integrated using a lentiviral vector

(MDA-MB-231, HCC1569, MCF10A). In the case of transient transfection plasmid pX462 containing Cas9-D10A nickase was transfected along with two gRNAs for enhanced specificity. Lentiviral vectors were generated in HEK293T cells using pLenti-CRISPR V2 together with packaging plasmids psPAX2 and pMD2.G. Culture medium containing viral particles (48 and 96h after transfection) was used to infect target cells in the presence of 8mg/ml polybrene. After transduction or transfection cells were puromycin-selected (0.5 – 3.0μg/ml) for 72h or 24h respectively, and subsequently clones picked and expanded. Clones were genotyped by sequencing of the targeted region and knock-out verified by immunoblotting.

Image cytometry-based high-throughput siRNA screening—The high-throughput siRNA screen was performed as previously described[83]. Briefly, HCC1569 breast cancer cells were transfected for 72 hours with a library of two individual siRNAs targeting 583 DNA repair genes (Silencer Select Human DNA Damage Response siRNA Library). Cells were then pulse-labelled for 1 hour with 10μM BrdU and then for 3 hours with 10μM Edu. Between the two pulse labels, the cells were treated with 2μM APH for 16h. Cells were fixed in 90% methanol overnight and then permeabilized with 0.3% Triton-X in PBS for 10 min. Incorporated EdU was detected using the Click-it Kit according to the manufacturer's instructions. The cells were then treated with 1% BSA and 2N HCl in PBS for 20min and stained for BrdU using anti-BrdU antibody diluted 1:400 in PBS for 1h followed by secondary anti-mouse antibody labelled with Alexa Fluor 488 dye diluted 1:200 in PBS for 30min. The genomic DNA was stained with Hoechst33342.

Flow cytometry—S-phase cell population and progression were studied by pulsing cells with 10μM EdU for 1h and releasing for the times indicated, then fixing in 80% v/v cold ethanol and subsequent staining using Click-it chemistry and Hoechst33342 stain according to the manufacturer's instructions, alternatively staining with Hoechst33342 alone to assess DNA content only. Stained cells were analysed on FACS Canto II flow cytometer and FACS Diva software (BD).

DNA fibre assays—Replication fork progression and/or restart were measured as described previously[84]. Briefly, cells were sequentially pulsed with 25μM CldU for 20 min, when applicable replication was blocked with APH (2μM) or HU (0.2mM), followed by wash-out and 250μM IdU pulse for 20–40 min. In between these incubation steps cells were washed twice with warm PBS. After harvesting, cell suspension was spotted onto a microscope slide, air-dried for 5 min, lysed and DNA fibres allowed to stretch by tilting the slide. Then, DNA fibres were fixed in methanol/acetic acid and denatured in 2M HCl. After thorough washing anti-CldU antibodies (BrdU antibody, Abcam, ab6326), anti-IdU antibodies (BrdU antibody, BD, 347580) and appropriate isotype-specific secondary antibodies coupled to Alexa-555 and Alexa-488 were used to detect labelled fibres. Images were taken using a Zeiss LSM880 confocal laser-scanning microscope and analysed using ImageJ software.

Cell proliferation and senescence assays—Proliferation rates were measured by plating cells in a 96-well format followed by respective cell treatment. Subsequently,

proliferation was either assessed by adding alamar blue and measuring fluorescence changes at 590nm indicative of cell proliferation. Alternatively, cells were fixed by methanol at the indicated time points and stained with 0.5 % w/v crystal violet solution. Subsequently, crystal violet was resolubilised in 50% v/v methanol / 5% v/v acetic acid and absorbance measured at 590nm using a SpectraMax M2e spectrophotometer (Molecular devices). To assess long-term proliferation rates in response to drug treatment a low number of cells (20 000–40 000/well) was plated on 6-well plates treated for 72h and allowed to recover in the absence of the drug for 10–14 days. Colonies were stained by crystal violet as above and images taken using CanoScan Lide 700f scanner (Canon).

Senescence was assessed by SA-βgal staining as described previously[85]. Briefly, cells were plated on 6-well plates, treated as indicated, subsequently fixed in 4% paraformaldehyde for 5min, then incubated at 37°C for 12 to 24h in staining solution containing 1mg/ml X-gal. Images were taken on a Leica DMI600 microscope and analysed using CellProfiler 4.2.1 software[80].

Mass spectrometry—Identification of FBXL12 interactors: Flp-In T-REx-293 cells stably expressing 3xHA-3xFLAG-FBXL12 or control cells were harvested and lysed in IP buffer consisting of 100mM Tris-HCl pH8.0, 150mM NaCl, 50mM EDTA, 0.1% NP-40, 10% glycerol, 1mM DTT, protease inhibitors, phosphatase inhibitors and DNase. Protein lysates were incubated with anti-HA agarose for 2 hours at 4°C. Beads were washed four times with IP buffer followed by washes with IP buffer lacking NP-40. Following the washes, bound protein complexes were eluted using 8M urea and 100mM Tris-HCl [pH 8.0]. Eluates were precipitated in acetone.

Acetone precipitates were resuspended in 100mM Tris-HCl [pH 8.5], 8M urea, reduced and alkylated using 5mM Tris (2-carboxyethyl) phosphine and 10mM iodoacetamide, respectively, and digested with Lys-C and trypsin. The digested peptides were subjected to offline high pH reverse phase fractionation using high pH reversed phase spin columns and subsequently analysed by LC-MS/MS. Peptides were separated by reversed phase chromatography using 75μm inner diameter fritted fused silica capillary column packed in-house to a length of 25 cm with Luna C18 3μm reverse phase particles. An increasing gradient of acetonitrile was delivered by a Thermo Scientific Dionex Ultimate 3000 at a flow rate of 300nl/min. MS/MS spectra were collected using data dependent acquisition on Orbitrap Fusion Lumos Tribrid mass spectrometer. Proteomic database search was performed using the MSGF+ algorithm via the target-decoy strategy against the EMBL Human reference proteome.

Network analysis of FBXL12 interactors was performed using evidence for physical protein interactions available through STRING-DB[86] with a STRING interaction score cut-off of 0.4. Identification of posttranslational FANCD2 modifications: MYC-tagged FANCD2 was immunoprecipitated as described above. On-bead reduction, alkylation and trypsin digestion were performed followed by SP3 peptide clean-up of the resulting supernatant[46]. Each sample was separated using a Thermo Scientific Dionex nano LC-system in a 3h 5–40% ACN gradient coupled to Thermo Scientific High Field QExactive. The software Proteome Discoverer 1.4 including Sequest-Percolator for improved identification was used to search

the Homo Sapiens Uniprot database for protein identification, limited to a false discovery rate of 1%.

Sub-cellular fractionation—Fractionation of cell lysates to distinguish chromatin-associated and soluble (nucleoplasm and cytoplasm) protein pools was carried out as previously described[87]. Briefly, cell suspension after harvesting was incubated in pre-extraction buffer (25mM HEPES [pH 7.4], 50mM NaCl, 1mM EDTA, 3mM $MgCl_2$, 300mM sucrose and 0.5% Triton X-100) for 5min under constant agitation, then spun down and supernatant soluble fraction collected. Remaining cell pellet was resolubilised in Laemmli buffer (4% SDS, 20% glycerol and 120 mM Tris [pH 6.8]), heated, sonicated and supernatant chromatin-enriched fraction collected after spin-down. Samples were analysed as described above.

Ubiquitination assays—*In vivo* and *in vitro* ubiquitination assays were performed as previously described[88]. Briefly, for *in vivo* ubiquitination HEK293T cells were treated with 10μM MG-132 for 4h prior to harvesting if indicated in the figure. Then, cells were lysed in NP40 lysis buffer, as above, additionally containing 1% SDS and 10mM N-ethylmaleimide (NEM), sonicated and heat-denatured at 95°C for 10min. Lysates were diluted and respective ubiquitination substrate immunoprecipitated followed by SDS-PAGE and immunoblotting analysis as above. To complement ubiquitination assays pulling down substrates, TUBES were used to pull down ubiquitin chains. For these assays SDS was omitted from the lysis buffer.

For *in vitro* ubiquitination assays, Dynabead-immobilised FANCD2 protein along with immunopurified and eluted SCF-FLAG-FBXL12 were resuspended in ubiquitination reaction buffer (25mM Tris–HCl pH 7.6, 5mM $MgCl_2$, 100mM NaCl) containing 2mM ATP, 1mM DTT, 200nM UBA1, 500nM HIS6-UBCH3 and 4μg ubiquitin. *In vitro* reactions were carried out at 37°C and incubated for 1h prior to three washes with NP40 lysis buffer and analysis by SDS-PAGE and immunoblotting.

In vitro phosphorylation and binding assays—FANCD2 constructs were in vitro transcribed and translated using the Promega coupled transcription/translation system according to the manufacturer's instructions. Translated proteins were then immunoprecipitated as above and after three additional washes with NP-40 lysis buffer (50mM Tris–HCl [pH 8.0], 150mM NaCl, 1% NP-40) incubated for 60min at 37°C in 50μl of phosphorylation buffer (50mM Tris–HCl [pH 7.4], 1mM EGTA, 150mM NaCl, 0.1% β-mercaptoethanol, 2mM ATP) with 1U of the respective recombinant kinase. For in vitro binding assays, bead-immobilised FANCD2 peptides or in vitro translated and phosphorylated FANCD2 protein constructs were resuspended in 50mM Tris–HCl [pH 7.4] and 150mM NaCl buffer in the presence of immunoprecipitated and eluted FLAG-FBXL12 and under constant gentle agitation at 4°C for 2h. Following incubation, the supernatant was aspirated and the beads washed three times with NP-40 lysis buffer prior to elution under reducing–denaturing conditions in SDS sample buffer at 95°C for 10min and SDS–PAGE as above.

Analysis of proteins on nascent DNA—Analysis of proteins on nascent DNA was performed based on a modified aniPOND (accelerated native isolation of protein on nascent DNA) protocol from Leung et al.[50]. Briefly, MDA-MB-231 or HEK293T cells (ca. 4 × 10e7 cells per condition) were pulse-labelled with 10μM EdU for the indicated times and then harvested or chased with medium containing 10μM thymidine for 90 min and harvested. Subsequently, nuclei were isolated in nuclei extraction buffer (20nM Hepes [pH 7.2], 50mM NaCl, 3mM $MgCl_2$, 300mM sucrose, 0.5% IGEPAL CA630) and biotin-azide click reactions performed under agitation for 1h at 4°C. Nuclei were lysed (lysis buffer: 25mM NaCl, 2mM EDTA, 50mM Tris-HCl [pH 8.0], 1% IGEPAL CA630 and protease inhibitors), chromatin sheared by sonication for 10s at maximum power using a Diagenode Bioruptor, followed by centrifugation and discarding of supernatant. These steps were repeated once to remove soluble and non-chromatin proteins. The remaining chromatin pellet was then resuspended in lysis buffer and sonicated for 12 rounds of 10s at maximum power to solubilise chromatin proteins. NaCl concentration of the final chromatin lysate was increased to physiological level by adding lysis buffer containing 150mM NaCl. 50μl of streptavidin beads per sample were used for streptavidin capture. Beads were washed three times and boiled in 1x SDS gel loading buffer prior to electrophoresis.

Immunofluorescence staining and microscopy—Cells were plated on cover slips and treated as appropriate for the respective experiment. Then, cells were fixed in 4% paraformaldehyde, permeabilised and blocked by 0.4% Triton-X 100 and 5% bovine serum albumin in TBS. Subsequently, they were incubated with the indicated antibodies in TBS containing 0.4% Triton-X 100 (TBS-T) for 2h, washed three times with TBS-T, incubated with appropriate isotype-specific secondary antibodies coupled to Alexa-555, Alexa-488 or Alexa-647 and Hoechst33342 stain. After three additional washes cover slips were mounted on slides in ProLong Diamond antifade mounting solution.

To stain UFBs cells were synchronised in anaphase using 9μM CDK1 inhibitor RO-3306 for 6h followed by a 45min wash-out with fresh medium. Cells were pre-extracted, fixed (described in detail in[89]) and stained as above.

Images were taken using a Zeiss LSM880 confocal laser-scanning microscope and analysed using ImageJ software.

For high-content imaging cells were plated in clear-bottom 96-well plates treated depending on the experimental question and subsequently stained analogously to cover slips as described above. After final washes cells were overlaid with PBS and imaged using ImageXpress μ automated microscope (Molecular devices). Resulting images were analysed using CellProfiler 4.2.1 and R 4.2.0[80,81].

For the single-cell replication recovery assay cells were sequentially pulsed with 10μM BrdU for 1h, replication was then blocked with APH (2μM), followed by wash-out and a 10μM EdU pulse for 1h. In between these incubation steps cells were washed twice with warm PBS. The replication block and final wash-out were carried out in the absence or presence of 1μM CDC7 inhibitor XL413 to assess the contribution of new origin firing.

Comet assays—Cell pellets (5×10^5 cells) were mixed with 200µl of 0.7% low melting point agarose, and then 65µl spotted onto an agarose precoated slide. After topping with a coverslip, slides were incubated at 4°C for 15 mins to solidify. Subsequently coverslips were removed and slides were placed in ice-cold lysis solution (2.5M NaCl, 100mM EDTA, 10mM Tris (pH 10]) 0.5% Triton X-100 and 1% N-lauroylsarcosine sodium salt) for 90 min. For alkaline comet assays, slides were incubated in electrophoresis buffer (200mM NaOH and 1mM disodium EDTA) with a pH of 13 for 1h at 4 °C. Next, slides were subjected to electrophoresis using the same buffer and a power supply voltage of 1V/cm for 30 min at 4 °C. Then, slides were gently washed twice with ddH2O and then fixed in 70% ethanol for 5 min at room temperature. For neutral comet assays, an electrophoresis buffer containing 100mM Tris base and 300mM sodium acetate was used instead. Following electrophoresis slides were immersed in DNA precipitation solution (1M ammonium acetate in ethanol) for 30 min at room temperature, and subsequently fixed as above. Fixed and dried slides were dyed with SYBRgreen solution for 15 min at room temperature and mounted with coverslips. Images were taken using the Zeiss LSM900-Airy confocal microscope. Finally, OpenComet software was used to analyse DNA breaks.

mRNA sequencing—RNA was extracted using the RNeasy Mini Kit. Sample quality was assessed using Agilent Technologies Bioanalyzer with Agilent RNA 6000 Nano Kit. RNA-seq was based on the Illumina NovaSeq 6000 platform and TruSeq library construction, with 60m pair-end reads per sample.

Gene-set enrichment analysis—Tools available through Galaxy Europe were used to test for gene sets within the Hallmark Collection of the Molecular Signatures Database that were up- or downregulated in relation to FBXL12 protein expression[90,91].

Quantitative real-time PCR—RNA was isolated using the RNeasy Mini Kit. 50 ng of purified RNA were then used for cDNA synthesis. Before preparing the PCR reaction, the cDNA was diluted 10 times and 4µl were used for each PCR reaction. Quantitative PCR was carried out in 96-well format on Thermo Scientific 7500 Fast Real-Time PCR System using SYBR green probes with the primers specified in the key resources table. Data were analysed using ΔΔCt method and presented as relative expression.

QUANTIFICATION AND STATISTICAL ANALYSIS

Data were analysed using GraphPad Prism 9. Unless noted otherwise in the figures or legends, results are representative of at least three biological independent replicates and presented as mean ± SD. Group-wise comparison was performed using unpaired Student’s t-test unless noted otherwise or for survival curves where the log-rank test was used. For correlations Spearman’s rank correlation coefficients and respective p-values are reported.

Supplementary Material

Refer to Web version on PubMed Central for supplementary material.

ACKNOWLEDGEMENTS

This research was funded by The Swedish Cancer Society, The Swedish Research Council, The Swedish Childhood Cancer Fund, Karolinska Institutet, Radiumhemmets Research Foundation and in part by the AstraZeneca-SLL-KI Open Innovation grant #18122013.

The authors acknowledge support from the National Genomics Infrastructure in Stockholm funded by Science for Life Laboratory, the Knut and Alice Wallenberg Foundation and SNIC/Uppsala Multidisciplinary Center for Advanced Computational Science, Jiri Bartek for providing CYCLIN E-inducible U2OS cells, the Fanconi anemia research fund for PD20 cells, and Nico Dantuma, Tony Huang, Didier Trono, Yue Xiong and Feng Zhang for plasmids. We are grateful to Jia Z. Shen, Steven I. Reed and Thomas Helleday for consultation and feedback.

REFERENCES

1. Macheret M, and Halazonetis TD (2015). DNA Replication Stress as a Hallmark of Cancer. Annual Review of Pathology: Mechanisms of Disease 10, 425–448. 10.1146/annurev-pathol-012414-040424.
2. Bartkova J, Rezaei N, Liontos M, Karakaidos P, Kletsas D, Issaeva N, Vassiliou L-VF, Kolettas E, Niforou K, Zoumpourlis VC, et al. (2006). Oncogene-induced senescence is part of the tumorigenesis barrier imposed by DNA damage checkpoints. Nature 444, 633–637. 10.1038/nature05268. [PubMed: 17136093]
3. Halazonetis TD, Gorgoulis VG, Bartek J, Magin S, Mladenov E, Helleday T, Haber JE, Iliakis G, Kallioniemi OP, and Halazonetis TD (2008). An Oncogene-Induced DNA Damage Model for Cancer Development. Science 319, 1352–1355. 10.1126/science.1140735. [PubMed: 18323444]
4. Kotsantis P, Silva LM, Irmscher S, Jones RM, Folkes L, Gromak N, and Petermann E (2016). Increased global transcription activity as a mechanism of replication stress in cancer. Nat Commun 7, 13087. 10.1038/ncomms13087. [PubMed: 27725641]
5. Kotsantis P, Petermann E, and Boulton SJ (2018). Mechanisms of Oncogene-Induced Replication Stress: Jigsaw Falling into Place. Cancer Discov 8, 537–555. 10.1158/2159-8290.cd-17-1461. [PubMed: 29653955]
6. Schoonen PM, Guerrero Llobet S, and van Vugt MATM (2019). Replication stress: Driver and therapeutic target in genomically instable cancers. In Advances in Protein Chemistry and Structural Biology (Academic Press Inc.), pp. 157–201. 10.1016/bs.apcsb.2018.10.006.
7. Gorski JW, Ueland FR, and Kolesar JM (2020). CCNE1 Amplification as a Predictive Biomarker of Chemotherapy Resistance in Epithelial Ovarian Cancer. Diagnostics 10, 279. 10.3390/diagnostics10050279. [PubMed: 32380689]
8. Guerrero Llobet S, van der Vegt B, Jongeneel E, Bense RD, Zwager MC, Schröder CP, Everts M, Fehrmann RSN, de Bock GH, and van Vugt MATM (2020). Cyclin E expression is associated with high levels of replication stress in triple-negative breast cancer. NPJ Breast Cancer 6, 40. 10.1038/s41523-020-00181-w. [PubMed: 32964114]
9. Schraml P, Bucher C, Bissig H, Nocito A, Haas P, Wilber K, Seelig S, Kononen J, Mihatsch MJ, Dirnhofer S, et al. (2003). Cyclin E overexpression and amplification in human tumours. J Pathol 200, 375–382. 10.1002/path.1356. [PubMed: 12845634]
10. Jones RM, Mortusewicz O, Afzal I, Lorvellec M, García P, Helleday T, and Petermann E (2013). Increased replication initiation and conflicts with transcription underlie Cyclin E-induced replication stress. Oncogene 32, 3744–3753. 10.1038/onc.2012.387. [PubMed: 22945645]
11. Bester AC, Roniger M, Oren YS, Im MM, Sarni D, Chaoat M, Bensimon A, Zamir G, Shewach DS, and Kerem B (2011). Nucleotide Deficiency Promotes Genomic Instability in Early Stages of Cancer Development. Cell 145, 435–446. 10.1016/j.cell.2011.03.044. [PubMed: 21529715]
12. Spruck CH, Won K-A, and Reed SI (1999). Deregulated cyclin E induces chromosome instability. Nature 401, 297–300. 10.1038/45836. [PubMed: 10499591]
13. Neelsen KJ, Zanini IMY, Herrador R, and Lopes M (2013). Oncogenes induce genotoxic stress by mitotic processing of unusual replication intermediates. Journal of Cell Biology 200, 699–708. 10.1083/jcb.201212058. [PubMed: 23479741]

14. Toledo LI, Murga M, Zur R, Soria R, Rodriguez A, Martinez S, Oyarzabal J, Pastor J, Bischoff JR, and Fernandez-Capetillo O (2011). A cell-based screen identifies ATR inhibitors with synthetic lethal properties for cancer-associated mutations. Nat Struct Mol Biol 18, 721–727. 10.1038/nsmb.2076. [PubMed: 21552262]

15. Garcia-Higuera I, Taniguchi T, Ganesan S, Meyn MS, Timmers C, Hejna J, Grompe M, and D'Andrea AD (2001). Interaction of the Fanconi Anemia Proteins and BRCA1 in a Common Pathway. Mol Cell 7, 249–262. 10.1016/S1097-2765(01)00173-3. [PubMed: 11239454]

16. Hussain S, Wilson JB, Medhurst AL, Hejna J, Witt E, Ananth S, Davies A, Masson JY, Moses R, West SC, et al. (2004). Direct interaction of FANCD2 with BRCA2 in DNA damage response pathways. Hum Mol Genet. 10.1093/hmg/ddh135.

17. Wang X, Andreassen PR, and D'Andrea AD (2004). Functional interaction of monoubiquitinated FANCD2 and BRCA2/FANCD1 in chromatin. Mol Cell Biol 24, 5850–5862. 10.1128/MCB.24.13.5850-5862.2004. [PubMed: 15199141]

18. Xu X, Xu Y, Guo R, Xu R, Fu C, Xing M, Sasanuma H, Li Q, Takata M, Takeda S, et al. (2021). Fanconi anemia proteins participate in a break-induced-replication-like pathway to counter replication stress. Nat Struct Mol Biol 28, 487–500. 10.1038/s41594-021-00602-9. [PubMed: 34117478]

19. Schlacher K, Wu H, and Jasin M (2012). A Distinct Replication Fork Protection Pathway Connects Fanconi Anemia Tumor Suppressors to RAD51-BRCA1/2. Cancer Cell 22, 106–116. 10.1016/j.ccr.2012.05.015. [PubMed: 22789542]

20. Chen YH, Jones MJK, Yin Y, Crist SB, Colnaghi L, Sims RJ, Rothenberg E, Jallepalli PV, and Huang TT (2015). ATR-Mediated Phosphorylation of FANCI Regulates Dormant Origin Firing in Response to Replication Stress. Mol Cell 58, 323–338. 10.1016/j.molcel.2015.02.031. [PubMed: 25843623]

21. Alcón P, Shakeel S, Chen ZA, Rappsilber J, Patel KJ, and Passmore LA (2020). FANCD2–FANCI is a clamp stabilized on DNA by monoubiquitination of FANCD2 during DNA repair. Nat Struct Mol Biol 27, 240–248. 10.1038/s41594-020-0380-1. [PubMed: 32066963]

22. Tan W, van Twest S, Leis A, Bythell-Douglas R, Murphy VJ, Sharp M, Parker MW, Crismani W, and Deans AJ (2020). Monoubiquitination by the human Fanconi anemia core complex clamps FANCI:FANCD2 on DNA in filamentous arrays. Elife 9. 10.7554/eLife.54128.

23. Wang R, Wang S, Dhar A, Peralta C, and Pavletich NP (2020). DNA clamp function of the monoubiquitinated Fanconi anaemia ID complex. Nature 580, 278–282. 10.1038/s41586-020-2110-6. [PubMed: 32269332]

24. van Twest S, Murphy VJ, Hodson C, Tan W, Swuec P, O'Rourke JJ, Heierhorst J, Crismani W, and Deans AJ (2017). Mechanism of Ubiquitination and Deubiquitination in the Fanconi Anemia Pathway. Mol Cell 65, 247–259. 10.1016/j.molcel.2016.11.005. [PubMed: 27986371]

25. Nijman SMB, Huang TT, Dirac AMG, Brummelkamp TR, Kerkhoven RM, D'Andrea AD, and Bernards R (2005). The deubiquitinating enzyme USP1 regulates the Fanconi anemia pathway. Mol Cell 17, 331–339. 10.1016/j.molcel.2005.01.008. [PubMed: 15694335]

26. Strohmaier H, Spruck CH, Kaiser P, Won K.-A. a, Sangfelt O, and Reed SI (2001). Human F-box protein hCdc4 targets cyclin E for proteolysis and is mutated in a breast cancer cell line. Nature 413, 316–322. 10.1038/35095076. [PubMed: 11565034]

27. Toledo LI, Altmeyer M, Rask M-B, Lukas C, Larsen DH, Povlsen LK, Bekker-Jensen S, Mailand N, Bartek J, and Lukas J (2013). ATR Prohibits Replication Catastrophe by Preventing Global Exhaustion of RPA. Cell 155, 1088–1103. 10.1016/j.cell.2013.10.043. [PubMed: 24267891]

28. Macheret M, and Halazonetis TD (2018). Intragenic origins due to short G1 phases underlie oncogene-induced DNA replication stress. Nature 555, 112–116. 10.1038/nature25507. [PubMed: 29466339]

29. Tsherniak A, Vazquez F, Montgomery PG, Weir BA, Kryukov G, Cowley GS, Gill S, Harrington WF, Pantel S, Krill-Burger JM, et al. (2017). Defining a Cancer Dependency Map. Cell 170, 564–576.e16. 10.1016/j.cell.2017.06.010. [PubMed: 28753430]

30. Hanada K, Budzowska M, Davies SL, van Drunen E, Onizawa H, Beverloo HB, Maas A, Essers J, Hickson ID, and Kanaar R (2007). The structure-specific endonuclease Mus81 contributes to

replication restart by generating double-strand DNA breaks. Nat Struct Mol Biol 14, 1096–1104. 10.1038/nsmb1313. [PubMed: 17934473]

31. Petermann E, and Helleday T (2010). Pathways of mammalian replication fork restart. Nat Rev Mol Cell Biol 11, 683–687. 10.1038/nrm2974. [PubMed: 20842177]
32. Rajagopalan H, Jallepalli PV, Rago C, Velculescu VE, Kinzler KW, Vogelstein B, and Lengauer C (2004). Inactivation of hCDC4 can cause chromosomal instability. Nature 428, 77–81. 10.1038/nature02313. [PubMed: 14999283]
33. Macheret M, Bhowmick R, Sobkowiak K, Padayachy L, Mailler J, Hickson ID, and Halazonetis TD (2020). High-resolution mapping of mitotic DNA synthesis regions and common fragile sites in the human genome through direct sequencing. Cell Res 30, 997–1008. 10.1038/s41422-020-0358-x. [PubMed: 32561860]
34. Minocherhomji S, Ying S, Bjerregaard VA, Bursomanno S, Aleliunaite A, Wu W, Mankouri HW, Shen H, Liu Y, and Hickson ID (2015). Replication stress activates DNA repair synthesis in mitosis. Nature 528, 286–290. 10.1038/nature16139. [PubMed: 26633632]
35. Glover TW, Wilson TE, and Arlt MF (2017). Fragile sites in cancer: more than meets the eye. Nat Rev Cancer 17, 489–501. 10.1038/nrc.2017.52. [PubMed: 28740117]
36. Ceccaldi R, Sarangi P, and D'Andrea AD (2016). The Fanconi anaemia pathway: new players and new functions. Nat Rev Mol Cell Biol 17, 337–349. 10.1038/nrm.2016.48. [PubMed: 27145721]
37. Mailand N, Bekker-Jensen S, Faustrup H, Melander F, Bartek J, Lukas C, and Lukas J (2007). RNF8 Ubiquitylates Histones at DNA Double-Strand Breaks and Promotes Assembly of Repair Proteins. Cell 131, 887–900. 10.1016/j.cell.2007.09.040. [PubMed: 18001824]
38. McKenna E, Traganos F, Zhao H, and Darzynkiewicz Z (2012). Persistent DNA damage caused by low levels of mitomycin C induces irreversible cell senescence. Cell Cycle. 10.4161/cc.21506.
39. Knipscheer P, Räschle M, Smogorzewska A, Enoiu M, Ho TV, Schärer OD, Elledge SJ, and Walter JC (2009). The fanconi anemia pathway promotes replication-dependent DNA interstrand cross-link repair. Science (1979). 10.1126/science.1182372.
40. Sato K, Shimomuki M, Katsuki Y, Takahashi D, Kobayashi W, Ishiai M, Miyoshi H, Takata M, and Kurumizaka H (2016). FANCI-FANCD2 stabilizes the RAD51-DNA complex by binding RAD51 and protects the 5′-DNA end. Nucleic Acids Res 44, 10758–10771. 10.1093/nar/gkw876. [PubMed: 27694619]
41. Wang Z, Liu P, Inuzuka H, and Wei W (2014). Roles of F-box proteins in cancer. Nat Rev Cancer 14, 233–247. 10.1038/nrc3700. [PubMed: 24658274]
42. Hornbeck PV, Zhang B, Murray B, Kornhauser JM, Latham V, and Skrzypek E (2015). PhosphoSitePlus, 2014: mutations, PTMs and recalibrations. Nucleic Acids Res 43, D512–D520. 10.1093/nar/gku1267. [PubMed: 25514926]
43. Samaras P, Schmidt T, Frejno M, Gessulat S, Reinecke M, Jarzab A, Zecha J, Mergner J, Giansanti P, Ehrlich H-C, et al. (2019). ProteomicsDB: a multi-omics and multi-organism resource for life science research. Nucleic Acids Res 48, D1153–D1163. 10.1093/nar/gkz974.
44. Guharoy M, Bhowmick P, Sallam M, and Tompa P (2016). Tripartite degrons confer diversity and specificity on regulated protein degradation in the ubiquitin-proteasome system. Nat Commun 7, 10239. 10.1038/ncomms10239. [PubMed: 26732515]
45. Brunner A, Suryo Rahmanto A, Johansson H, Franco M, Viiliäinen J, Gazi M, Frings O, Fredlund E, Spruck C, Lehtiö J, et al. (2020). PTEN and DNA-PK determine sensitivity and recovery in response to WEE1 inhibition in human breast cancer. Elife 9. 10.7554/eLife.57894.
46. Moggridge S, Sorensen PH, Morin GB, and Hughes CS (2018). Extending the Compatibility of the SP3 Paramagnetic Bead Processing Approach for Proteomics. J Proteome Res 17, 1730–1740. 10.1021/acs.jproteome.7b00913. [PubMed: 29565595]
47. Fernandez-Vidal A, Vignard J, and Mirey G (2017). Around and beyond 53BP1 nuclear bodies. Int J Mol Sci. 10.3390/ijms18122611.
48. Aarts M, Sharpe R, Garcia-Murillas I, Gevensleben H, Hurd MS, Shumway SD, Toniatti C, Ashworth A, and Turner NC (2012). Forced Mitotic Entry of S-Phase Cells as a Therapeutic Strategy Induced by Inhibition of WEE1. Cancer Discov 2, 524–539. 10.1158/2159-8290.CD-11-0320. [PubMed: 22628408]

49. Fu S, Wang Y, Keyomarsi K, and Meric-Bernstein F (2018). Strategic development of AZD1775, a Wee1 kinase inhibitor, for cancer therapy. Expert Opin Investig Drugs 27, 741–751. 10.1080/13543784.2018.1511700.
50. Leung KHT, El Hassan MA, and Bremner R (2013). A rapid and efficient method to purify proteins at replication forks under native conditions. Biotechniques 55, 204–206. 10.2144/000114089. [PubMed: 24107252]
51. Sijacki T, Alcón P, Chen ZA, McLaughlin SH, Shakeel S, Rappsilber J, and Passmore LA (2022). The DNA-damage kinase ATR activates the FANCD2-FANCI clamp by priming it for ubiquitination. Nat Struct Mol Biol 29, 881–890. 10.1038/s41594-022-00820-9. [PubMed: 36050501]
52. Timmers C, Taniguchi T, Hejna J, Reifsteck C, Lucas L, Bruun D, Thayer M, Cox B, Olson S, D'Andrea AD, et al. (2001). Positional Cloning of a Novel Fanconi Anemia Gene, FANCD2. Mol Cell 7, 241–248. 10.1016/S10972765(01)00172-1. [PubMed: 11239453]
53. Johansson HJ, Socciarelli F, Vacanti NM, Haugen MH, Zhu Y, Siavelis I, Fernandez-Woodbridge A, Aure MR, Sennblad B, Vesterlund M, et al. (2019). Breast cancer quantitative proteome and proteogenomic landscape. Nat Commun 10, 1600. 10.1038/s41467-019-09018-y. [PubMed: 30962452]
54. Lehtiö J, Arslan T, Siavelis I, Pan Y, Socciarelli F, Berkovska O, Umer HM, Mermelekas G, Pirmoradian M, Jönsson M, et al. (2021). Proteogenomics of non-small cell lung cancer reveals molecular subtypes associated with specific therapeutic targets and immune-evasion mechanisms. Nat Cancer. 10.1038/s43018-021-00259-9.
55. Weinstein JN, Collisson EA, Mills GB, Shaw KRM, Ozenberger BA, Ellrott K, Shmulevich I, Sander C, and Stuart JM (2013). The Cancer Genome Atlas PanCancer analysis project. Nat Genet 45, 1113–1120. 10.1038/ng.2764. [PubMed: 24071849]
56. McGrail DJ, Lin CC-J, Dai H, Mo W, Li Y, Stephan C, Davies P, Lu Z, Mills GB, Lee J-S, et al. (2018). Defective Replication Stress Response Is Inherently Linked to the Cancer Stem Cell Phenotype. Cell Rep 23, 2095–2106. 10.1016/j.celrep.2018.04.068. [PubMed: 29768207]
57. Nayak S, Calvo JA, Cong K, Peng M, Berthiaume E, Jackson J, Zaino AM, Vindigni A, Hadden MK, and Cantor SB (2020). Inhibition of the translesion synthesis polymerase REV1 exploits replication gaps as a cancer vulnerability. Sci Adv 6, eaaz7808. 10.1126/sciadv.aaz7808. [PubMed: 32577513]
58. Cong K, Peng M, Kousholt AN, Lee WTC, Lee S, Nayak S, Krais J, VanderVere-Carozza PS, Pawelczak KS, Calvo J, et al. (2021). Replication gaps are a key determinant of PARP inhibitor synthetic lethality with BRCA deficiency. Mol Cell 81, 3128–3144.e7. 10.1016/j.molcel.2021.06.011. [PubMed: 34216544]
59. Kim JM, Parmar K, Huang M, Weinstock DM, Ruit CA, Kutok JL, and D'Andrea AD (2009). Inactivation of Murine Usp1 Results in Genomic Instability and a Fanconi Anemia Phenotype. Dev Cell 16, 314–320. 10.1016/j.devcel.2009.01.001. [PubMed: 19217432]
60. Arkinson C, Chaugule VK, Toth R, and Walden H (2018). Specificity for deubiquitination of monoubiquitinated FANCD2 is driven by the N-terminus of USP1. Life Sci Alliance 1, e201800162. 10.26508/lsa.201800162. [PubMed: 30456385]
61. Gibbs-Seymour I, Oka Y, Rajendra E, Weinert BT, Passmore LA, Patel KJ, Olsen JV, Choudhary C, Bekker-Jensen S, and Mailand N (2015). UbiquitinSUMO circuitry controls activated fanconi anemia ID complex dosage in response to DNA damage. Mol Cell 57, 150–164. 10.1016/j.molcel.2014.12.001. [PubMed: 25557546]
62. Clark DW, Tripathi K, Dorsman JC, and Palle K (2015). FANCJ protein is important for the stability of FANCD2/FANCI proteins and protects them from proteasome and caspase-3 dependent degradation. Oncotarget 6, 28816–28832. 10.18632/oncotarget.5006. [PubMed: 26336824]
63. Syljuåsen RG, Sørensen CS, Hansen LT, Fugger K, Lundin C, Johansson F, Helleday T, Sehested M, Lukas J, and Bartek J (2005). Inhibition of Human Chk1 Causes Increased Initiation of DNA Replication, Phosphorylation of ATR Targets, and DNA Breakage. Mol Cell Biol 25, 3553–3562. 10.1128/MCB.25.9.3553-3562.2005. [PubMed: 15831461]
64. Sanjiv K, Hagenkort A, Calderón-Montaño JM, Koolmeister T, Reaper PM, Mortusewicz O, Jacques SA, Kuiper RV, Schultz N, Scobie M, et al. (2016). Cancer-Specific Synthetic Lethality

between ATR and CHK1 Kinase Activities. Cell Rep 14, 298–309. 10.1016/j.celrep.2015.12.032. [PubMed: 26748709]

65. González Besteiro MA, Calzetta NL, Loureiro SM, Habif M, Bétous R, Pillaire M-J, Maffia A, Sabbioneda S, Hoffmann J-S, and Gottifredi V (2019). Chk1 loss creates replication barriers that compromise cell survival independently of excess origin firing. EMBO J 38, e101284. 10.15252/embj.2018101284. [PubMed: 31294866]
66. Pettitt SJ, Krastev DB, Brandsma I, Dréan A, Song F, Aleksandrov R, Harrell MI, Menon M, Brough R, Campbell J, et al. (2018). Genome-wide and high-density CRISPR-Cas9 screens identify point mutations in PARP1 causing PARP inhibitor resistance. Nat Commun 9, 1849. 10.1038/s41467-018-03917-2. [PubMed: 29748565]
67. Foulkes WD, Brunet J-S, Stefansson IM, Straume O, Chappuis PO, Bégin LR, Hamel N, Goffin JR, Wong N, Trudel M, et al. (2004). The prognostic implication of the basal-like (cyclin E high/p27 low/p53+/glomeruloid-microvascular-proliferation+) phenotype of BRCA1-related breast cancer. Cancer Res 64, 830–835. [PubMed: 14871808]
68. Keyomarsi K, Tucker SL, Buchholz TA, Callister M, Ding Y, Hortobagyi GN, Bedrosian I, Knickerbocker C, Toyofuku W, Lowe M, et al. (2002). Cyclin E and Survival in Patients with Breast Cancer. New England Journal of Medicine 347, 1566–1575. 10.1056/NEJMoa021153. [PubMed: 12432043]
69. Yeh C-H, Bellon M, and Nicot C (2018). FBXW7: a critical tumor suppressor of human cancers. Mol Cancer 17, 115. 10.1186/s12943-018-0857-2. [PubMed: 30086763]
70. Chen X, Low K-H, Alexander A, Jiang Y, Karakas C, Hess KR, Carey JPW, Bui TN, Vijayaraghavan S, Evans KW, et al. (2018). Cyclin E Overexpression Sensitizes Triple-Negative Breast Cancer to Wee1 Kinase Inhibition. Clinical Cancer Research 24, 6594–6610. 10.1158/1078-0432.CCR-18-1446. [PubMed: 30181387]
71. Chen X, Yang D, Carey JPW, Karakas C, Albarracin C, Sahin AA, Arun BK, Guray Durak M, Li M, Kohansal M, et al. (2021). Targeting Replicative Stress and DNA Repair by Combining PARP and Wee1 Kinase Inhibitors Is Synergistic in Triple Negative Breast Cancers with Cyclin E or BRCA1 Alteration. Cancers (Basel) 13, 1656. 10.3390/cancers13071656. [PubMed: 33916118]
72. Murga M, Campaner S, Lopez-Contreras AJ, Toledo LI, Soria R, Montaña MF, D'Artista L, Schleker T, Guerra C, Garcia E, et al. (2011). Exploiting oncogene-induced replicative stress for the selective killing of Myc-driven tumors. Nat Struct Mol Biol 18, 1331–1335. 10.1038/nsmb.2189. [PubMed: 22120667]
73. Jakobs PM, Sahaayaruban P, Saito H, Reifsteck C, Olson S, Joenje H, Moses RE, and Grompe M (1996). Immortalization of four new fanconi anemia fibroblast cell lines by an improved procedure. Somat Cell Mol Genet 22, 151–157. 10.1007/BF02369905. [PubMed: 8782494]
74. Meetei AR, De Winter JP, Medhurst AL, Wallisch M, Waisfisz Q, van de Vrugt HJ, Oostra AB, Yan Z, Ling C, Bishop CE, et al. (2003). A novel ubiquitin ligase is deficient in Fanconi anemia. Nat Genet 35, 165–170. 10.1038/ng1241. [PubMed: 12973351]
75. Ran FA, Hsu PD, Wright J, Agarwala V, Scott DA, and Zhang F (2013). Genome engineering using the CRISPR-Cas9 system. Nat Protoc 8, 2281–2308. 10.1038/nprot.2013.143. [PubMed: 24157548]
76. Sanjana NE, Shalem O, and Zhang F (2014). Improved vectors and genome-wide libraries for CRISPR screening. Nat Methods 11, 783–784. 10.1038/nmeth.3047. [PubMed: 25075903]
77. Furukawa M, Zhang Y, McCarville J, Ohta T, and Xiong Y (2000). The CUL1 C-Terminal Sequence and ROC1 Are Required for Efficient Nuclear Accumulation, NEDD8 Modification, and Ubiquitin Ligase Activity of CUL1. Mol Cell Biol 20, 8185–8197. 10.1128/MCB.20.21.8185-8197.2000. [PubMed: 11027288]
78. Kamitani T, Kito K, Nguyen HP, and Yeh ETH (1997). Characterization of NEDD8, a Developmentally Down-regulated Ubiquitin-like Protein. Journal of Biological Chemistry 272, 28557–28562. 10.1074/jbc.272.45.28557. [PubMed: 9353319]
79. Dantuma NP, Groothuis TAM, Salomons FA, and Neefjes J (2006). A dynamic ubiquitin equilibrium couples proteasomal activity to chromatin remodeling. Journal of Cell Biology 173, 19–26. 10.1083/jcb.200510071. [PubMed: 16606690]

80. Carpenter AE, Jones TR, Lamprecht MR, Clarke C, Kang I, Friman O, Guertin DA, Chang J, Lindquist RA, Moffat J, et al. (2006). CellProfiler: image analysis software for identifying and quantifying cell phenotypes. Genome Biol 7, R100. 10.1186/gb-2006-7-10-r100. [PubMed: 17076895]
81. R Development Core Team (2016). R: A language and environment for statistical computing. R Foundation for Statistical Computing. 10.1017/CBO9781107415324.004.
82. Jordan M, Schallhorn A, and Wurm FM (1996). Transfecting Mammalian Cells: Optimization of Critical Parameters Affecting Calcium-Phosphate Precipitate Formation. Nucleic Acids Res 24, 596–601. 10.1093/nar/24.4.596. [PubMed: 8604299]
83. Costantino L, Sotiriou SK, Rantala JK, Magin S, Mladenov E, Helleday T, Haber JE, Iliakis G, Kallioniemi OP, and Halazonetis TD (2014). Break-induced replication repair of damaged forks induces genomic duplications in human cells. Science 343, 88–91. 10.1126/science.1243211. [PubMed: 24310611]
84. Nieminuszczy J, Schwab RA, and Niedzwiedz W (2016). The DNA fibre technique – tracking helicases at work. Methods 108, 92–98. 10.1016/j.ymeth.2016.04.019. [PubMed: 27102626]
85. Debacq-Chainiaux F, Erusalimsky JD, Campisi J, and Toussaint O (2009). Protocols to detect senescence-associated beta-galactosidase (SA-betagal) activity, a biomarker of senescent cells in culture and in vivo. Nat Protoc 4, 1798–1806. 10.1038/nprot.2009.191. [PubMed: 20010931]
86. Szklarczyk D, Gable AL, Lyon D, Junge A, Wyder S, Huerta-Cepas J, Simonovic M, Doncheva NT, Morris JH, Bork P, et al. (2019). STRING v11: protein–protein association networks with increased coverage, supporting functional discovery in genome-wide experimental datasets. Nucleic Acids Res 47, D607–D613. 10.1093/nar/gky1131. [PubMed: 30476243]
87. Peña-Diaz J, Bregenhorn S, Ghodgaonkar M, Follonier C, Artola-Borán M, Castor D, Lopes M, Sartori AA, and Jiricny J (2012). Noncanonical Mismatch Repair as a Source of Genomic Instability in Human Cells. Mol Cell 47, 669–680. 10.1016/j.molcel.2012.07.006. [PubMed: 22864113]
88. Suryo Rahmanto A, Savov V, Brunner A, Bolin S, Weishaupt H, Malyukova A, Rosén G, Čančer M, Hutter S, Sundström A, et al. (2016). FBW7 suppression leads to SOX9 stabilization and increased malignancy in medulloblastoma. EMBO J 35, 2192–2212. 10.15252/embj.201693889. [PubMed: 27625374]
89. Bizard AH, Nielsen CF, and Hickson ID (2018). Detection of Ultrafine Anaphase Bridges. In Methods in molecular biology (Clifton, N.J.), pp. 495–508. 10.1007/978-1-4939-7306-4_33.
90. Subramanian A, Tamayo P, Mootha VK, Mukherjee S, Ebert BL, Gillette MA, Paulovich A, Pomeroy SL, Golub TR, Lander ES, et al. (2005). Gene set enrichment analysis: A knowledge-based approach for interpreting genome-wide expression profiles. Proceedings of the National Academy of Sciences 102, 15545–15550. 10.1073/pnas.0506580102.
91. Liberzon A, Birger C, Thorvaldsdóttir H, Ghandi M, Mesirov JP, and Tamayo P (2015). The Molecular Signatures Database Hallmark Gene Set Collection. Cell Syst 1, 417–425. 10.1016/j.cels.2015.12.004. [PubMed: 26771021]

Highlights

- SCF^{FBXL12} poly-ubiquitinates and targets chromatin-bound FANCD2 for degradation.
- In the absence of FBXL12, FANCD2 becomes trapped, impeding replication progression.
- FANCD2 phosphodegron mutants fail to rescue fork progress under replication stress.
- FBXL12 represents a vulnerability of CYCLIN E-overexpressing cancer cells.

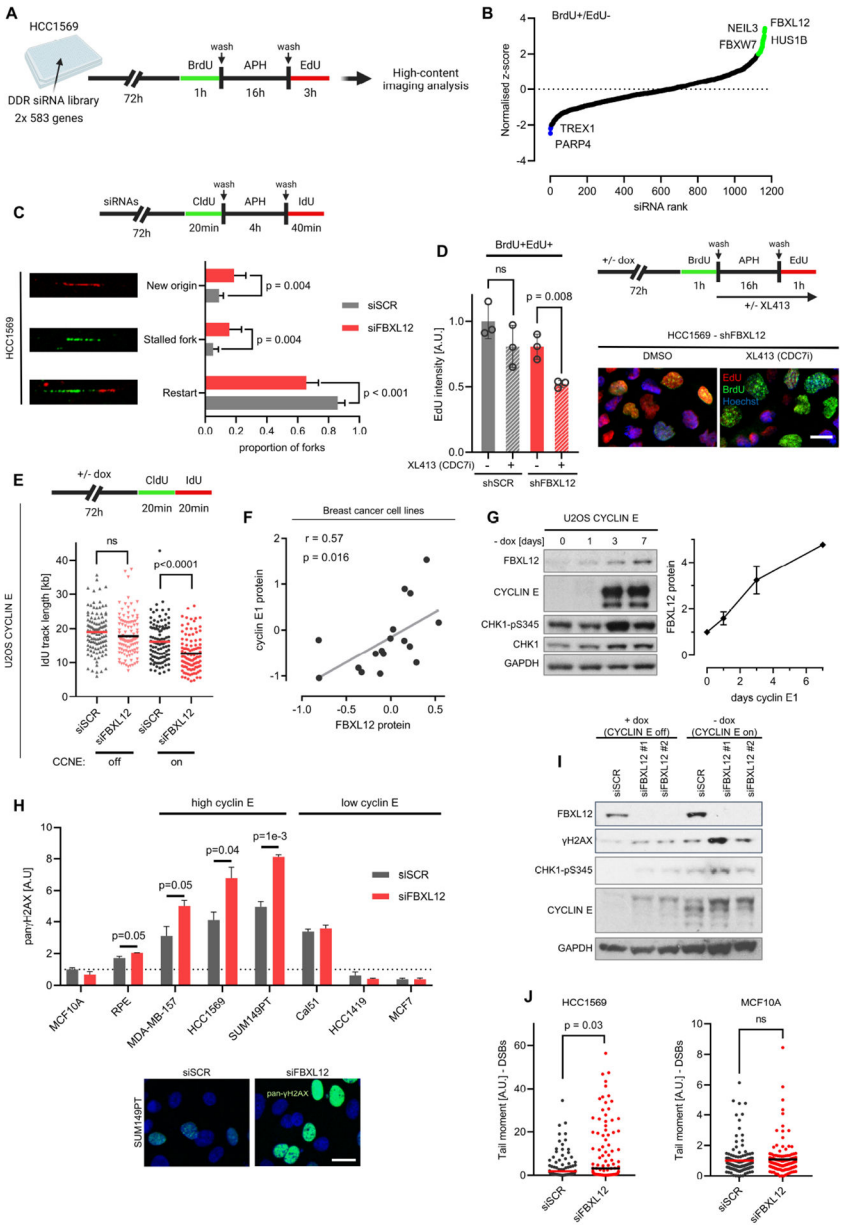

Fig. 1.

FBXL12 suppresses CYCLIN E-induced replication stress and facilitates replication recovery

A. Outline of the replication recovery screen in HCC1569 cells.

B. Top siRNA hits for the BrdU+/EdU− gate. FBXL12 and other selected top hits with z-scores above 2 or below −2 are highlighted.

C. DNA fibre assay comparing proportions of restarted, stalled and newly started (new origin) replication forks between control and FBXL12 knockdown in HCC1569 cells.

D. Single-cell replication recovery assay in HCC1569 control and dox-inducible shFBXL12-expressing cells. Red = EdU, blue = Hoechst33342, scale bar = 20μm.

E. Replication track lengths in U2OS CYCLIN E1 tet-off cells upon control or FBXL12 knockdown. Per condition a total of >100 replication tracks from two independent experiments were measured.

F. Correlation analysis between FBXL12 and CYCLIN E1 protein expression in a panel of 17 breast cancer cell lines. Log2-transformed protein ratio to mean is plotted.

G. Immunoblots and quantification of FBXL12 band intensities in U2OS CYCLIN E1 tet-off cells cultured in the absence of doxycycline for 0, 1, 3 and 7 days.

H. HCI-based quantification of pan-γH2AX-positive nuclei intensities in a panel of untransformed and breast cancer cell lines subdivided based on CYCLIN E expression. Intensities are plotted in arbitrary units [A.U.] and MCF10A cells (transfected with siSCR) used as baseline and set to 1. Green = γH2AX, blue = Hoechst33342, scale bar = 20μm.

I. Immunoblots of U2OS CYCLIN E1 tet-off cells upon control or FBXL12 knockdown.

J. Neutral comet assay of HCC1569 and MCF10A cells transfected with control or FBXL12-targeting siRNAs. Tail moment of >50 cells per condition is plotted.

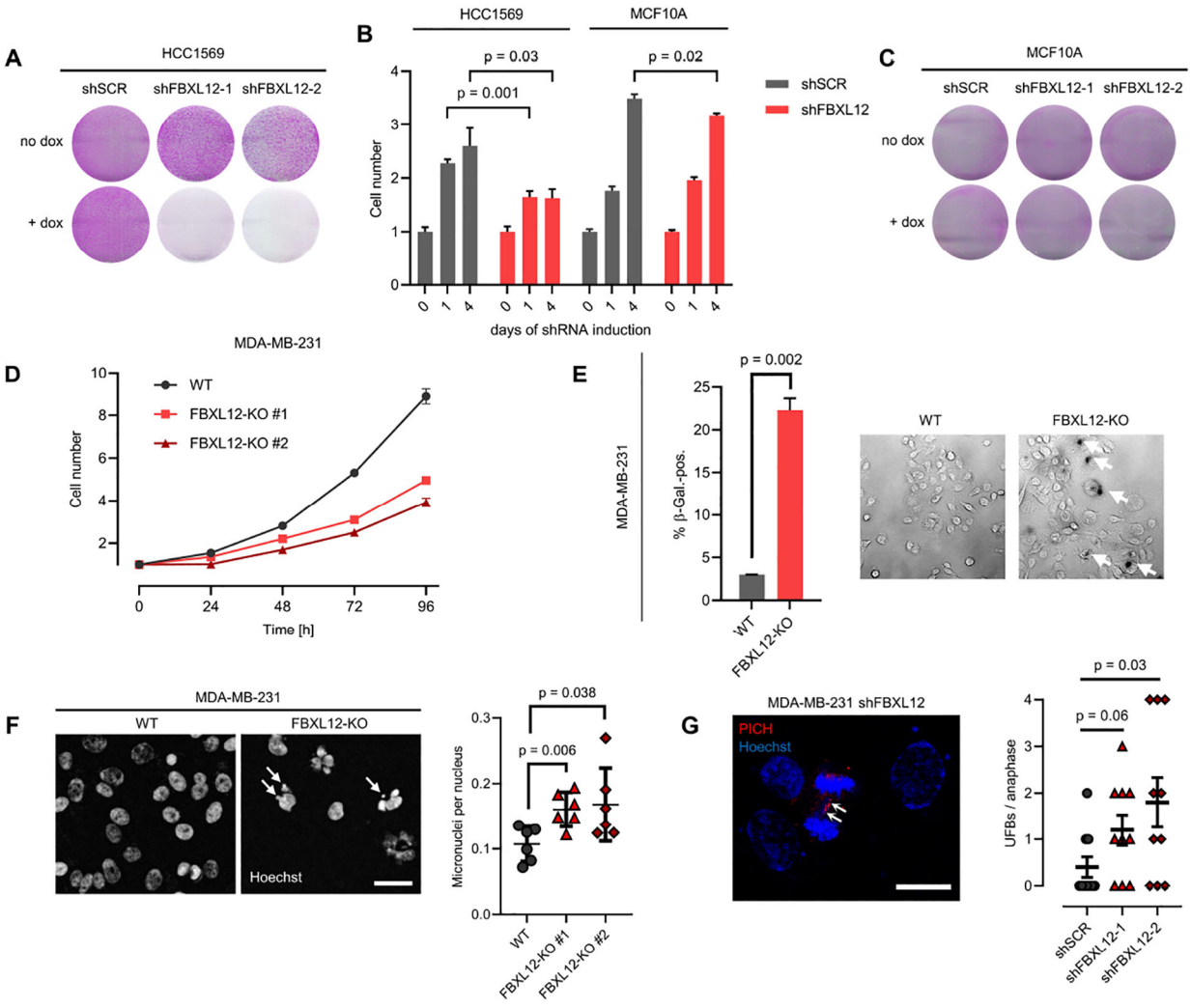

Fig. 2.

FBXL12 sustains genome stability and unimpeded proliferation in BLBC cells

A. Colony formation assay of HCC1569 control or shFBXL12 cells upon shRNA induction for 10 days.

B. Proliferation assays of HCC1569 and MCF10A shFBXL12 or control cells after 0, 1 and 4 days shRNA induction.

C. Colony formation assay as in panel A using MCF10A control and shFBXL12 cells.

D. 96h proliferation assay of MDA-MB-231-FBXL12-WT and two isogenic FBXL12-KO cell lines.

E. Proportions of SA-β-Gal-positive MDA-MB-231-FBXL12-WT and FBXL12-KO cells.

F. Micronuclei occurrence in MDA-MB-231-FBXL12-WT and FBXL12-KO cells measured by HCI. Arrows indicate micronuclei. Scale bar = 30μm.

G. UFBs in MDA-MB-231 shFBXL12 and control cells. Representative image of an MDA-MB-231 shFBXL12 cell in anaphase with white arrows indicating UFBs. Scale bar = 20μm.

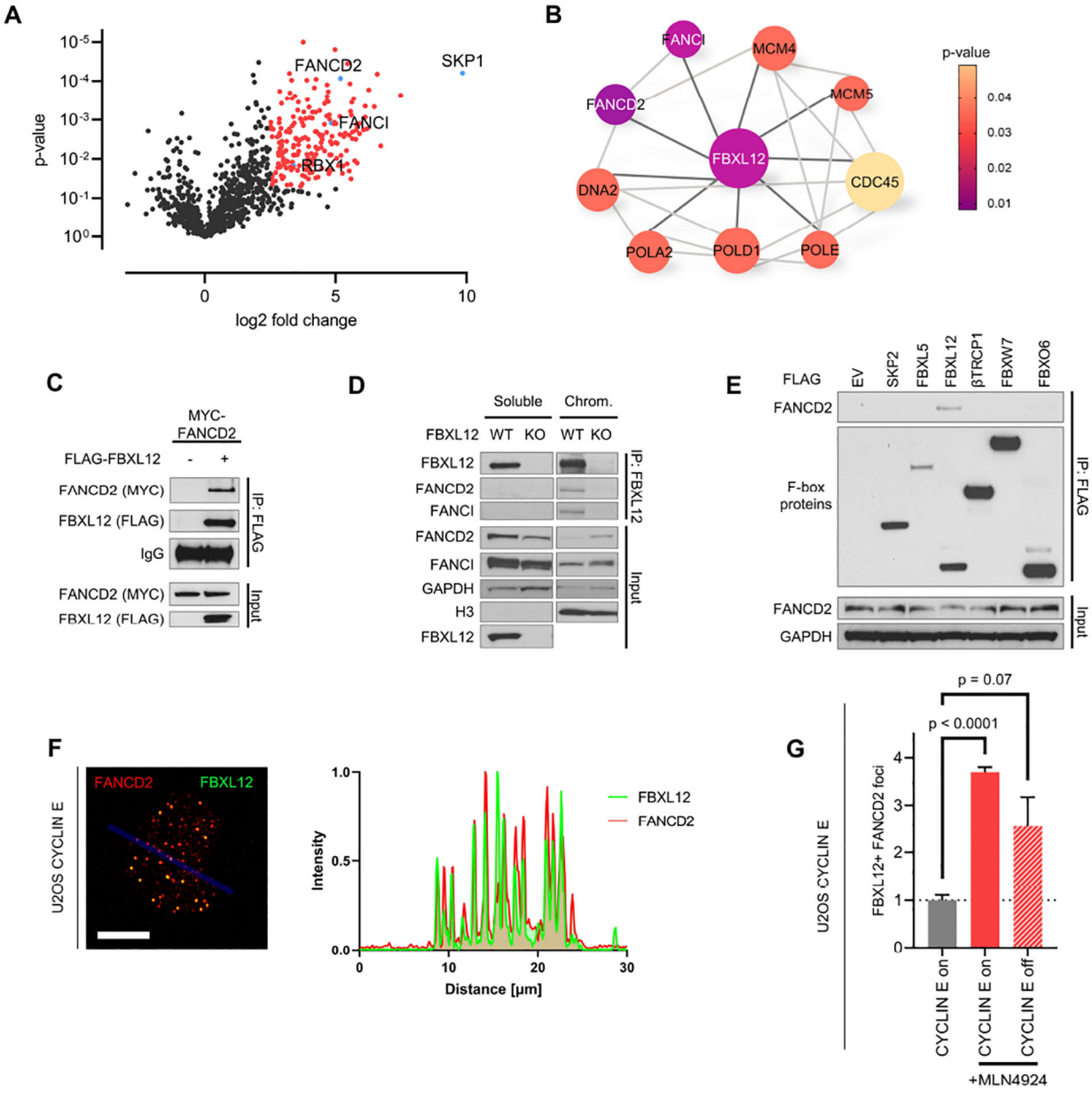

Fig. 3.

FBXL12 interacts with Fanconi anaemia proteins FANCD2 and FANCI

A. Proteomic mass spectrometry identification of FBXL12 interactors. Volcano plot showing log2-transformed fold enrichment of putative interactors on the x-axis and negative log-transformed p-values on the y-axis.

B. FANCD2-FANCI-associated subnetwork of identified FBXL12 interactors (with adjusted p-values < 0.05). Protein symbol sizes correspond to fold enrichment of interactors and colour-codes indicate the respective p-values.

C. Immunoprecipitation of FLAG-FBXL12 from HEK293 cell lysates.

D. Immunoprecipitation of endogenous FBXL12 from chromatin-associated and soluble (cytoplasm + nucleoplasm) lysate fractions of HEK293T FBXL12-WT and FBXL12-KO cells.

E. Immunoprecipitation of FLAG-tagged F-box proteins from HEK293T cell lysates to assess interaction with endogenous FANCD2.

F. Colocalization of endogenous FANCD2 and transiently expressed GFP-tagged FBXL12 in U2OS CYCLIN E cells. Representative MLN4924-treated cell with intensity plots of FBXL12 and FANCD2 signals along the indicated blue line. Scale bar = 10μm. Red = FANCD2; Green = FBXL12; Blue = Hoechst33342.

G. Quantification of FANCD2-FBXL12 double-positive foci per nucleus representative of three replicates with a minimum of 50 cells per condition. Values plotted are foci numbers relative to untreated control.

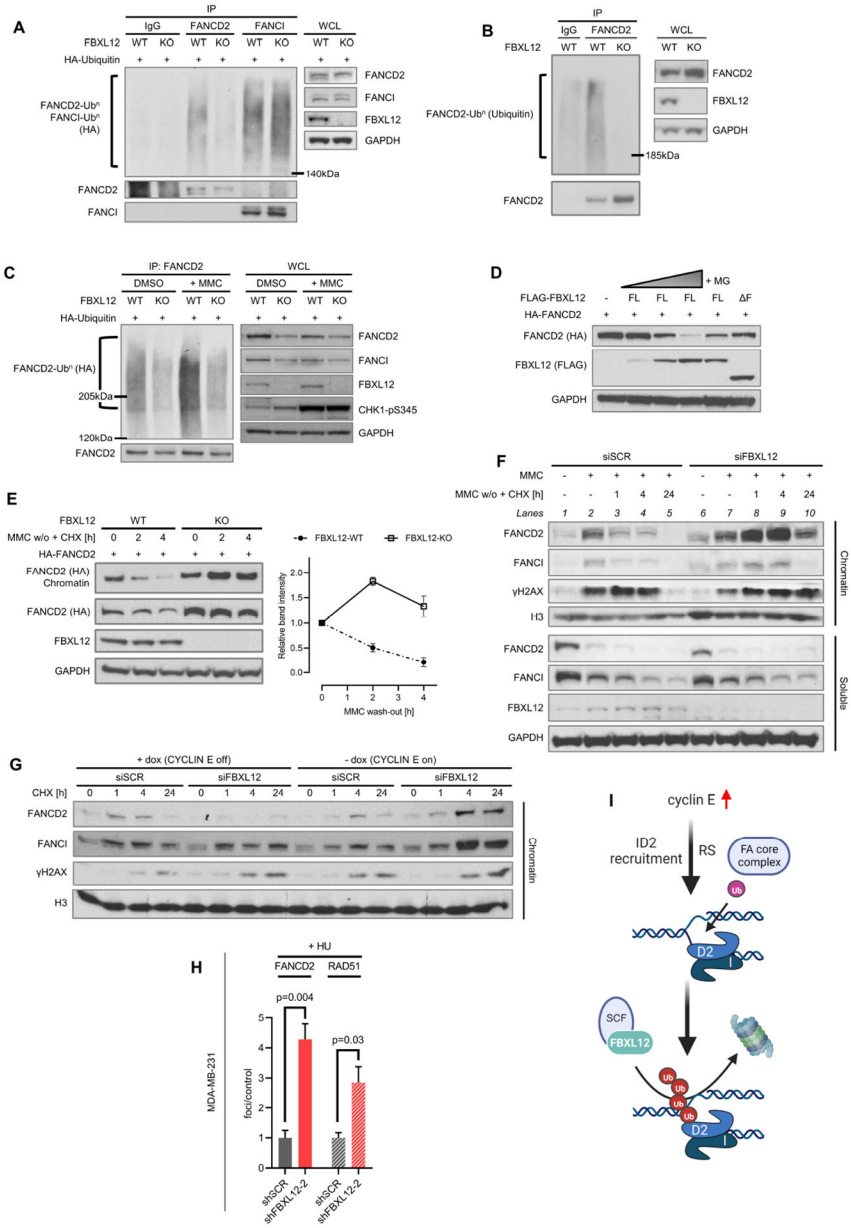

Fig. 4.

FBXL12 targets chromatin-associated FANCD2 for degradation

A. FANCD2 and FANCI *in vivo* ubiquitination assay under denaturing conditions in HEK293T FBXL12-WT and FBXL12-KO cells transfected with HA-Ubiquitin and treated with MG-132.

B. Endogenous FANCD2 ubiquitination in HEK293T FBXL12-WT and FBXL12-KO cells treated with MG-132.

C. *In vivo* ubiquitination assay of FANCD2 as in A ± 4h MMC treatment.

D. Immunoblots of HEK293T cells transfected with HA-FANCD2 and increasing amounts of FLAG-FBXL12-FL (full length) ± MG-132 treatment, or FLAG-FBXL12-ΔF.

E. HA-FANCD2 turnover after MMC-mediated stimulation (4h) of FA signalling and subsequent wash-out in HEK293T FBXL12-WT and FBXL12-KO cells.
F. Turnover of chromatin-associated and soluble FANCD2 after MMC wash-out as in E comparing control and siFBXL12-transfected RPE1 cells.
G. FANCD2 CHX chase in U2OS CYCLIN E cells upon control or siFBXL12 transfection, ± 72h doxycycline. Chromatin-associated fractions are shown here and soluble fractions in Fig. S5K.
H. FANCD2 and RAD51 foci in MDA-MB-231 control or shFBXL12 cells treated with HU for 16h. Data show mean from >200 cells and three replicates.
I. Visual summary of the CYCLIN E-FBXL12-FANCD2 axis.

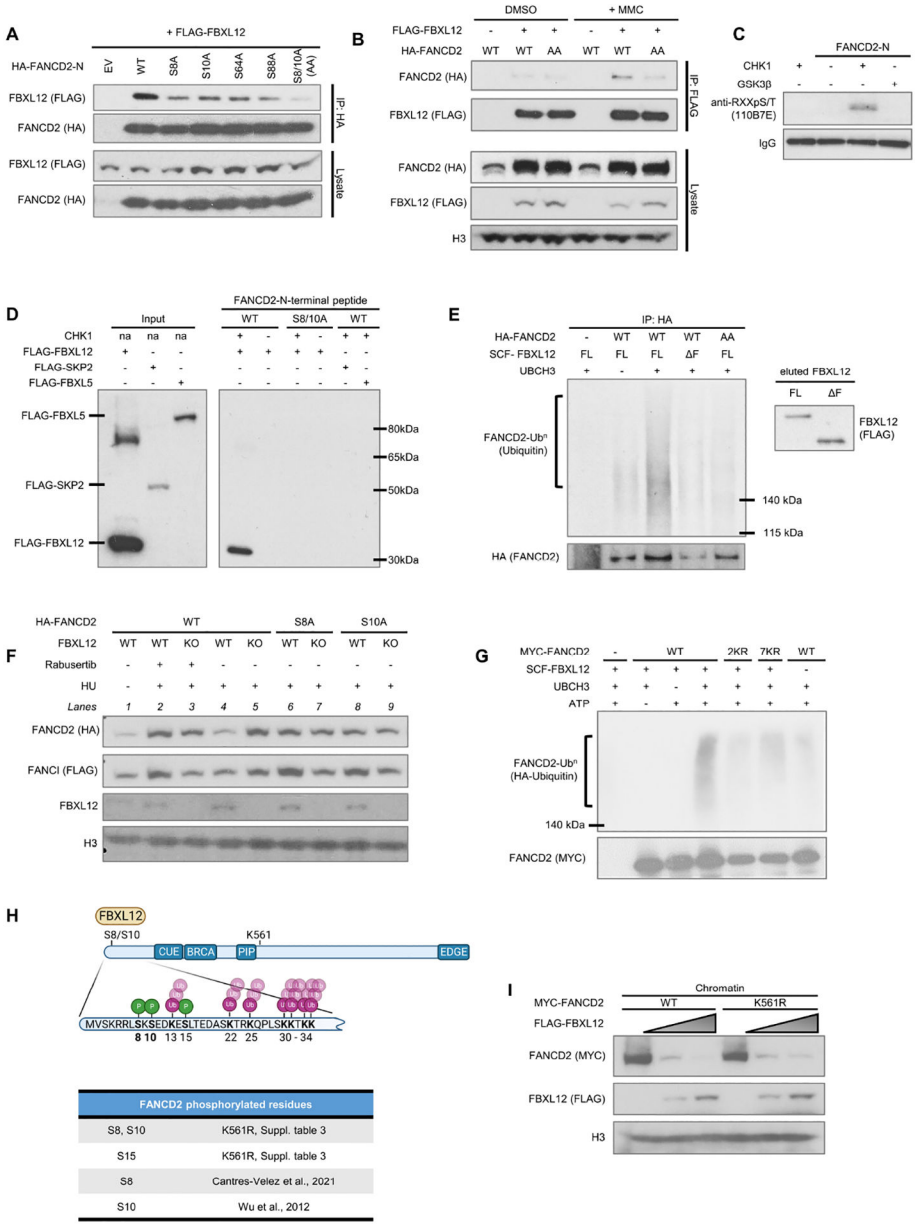

Fig. 5.

Phosphorylation of the FANCD2 N-terminus by CHK1 stimulates ubiquitination by FBXL12

A. Immunoprecipitation of HA-FANCD2-1-140 (FANCD2-N) constructs mutated at the indicated putative phosphorylation sites and transfected along with FLAG-FBXL12.

B. Immunoprecipitation of FLAG-FBXL12 from HEK293 cell lysates transfected with the indicated constructs and ± 4h MMC treatment.

C. Immunoblot of *in vitro* transcribed and translated FANCD2-N incubated ± recombinant CHK1 or GSK3β kinase.

D. *In vitro* phosphorylation by CHK1, and FBXL12 or control F-box protein binding assay with N-terminal FANCD2 peptides.

E. *In vitro* ubiquitination assay performed on immunopurified and immobilised HA-FANCD2-WT and HA-FANCD2-AA, using immunopurified and eluted FLAG-FBXL12-FL or -ΔF.

F. HEK293T FBXL12-WT and -KO cells were transfected with HA-FANCD2-WT, HA-FANCD2-S8A or S10A mutants, and incubated ± HU for 16h. Where indicated cells were additionally treated with CHK1 inhibitor Rabusertib for the last two hours.

G. *In vitro* ubiquitination assay performed on immunopurified and immobilised MYC-FANCD2-WT, 2KR, 7KR or AA mutant FANCD2, using immunopurified and eluted FLAG-FBXL12-FL.

H. Top: Schematic indicating major FANCD2 protein domains and an enlarged view of the N-terminal region containing the FBXL12 degron and identified phosphorylated and ubiquitinated residues. Bottom: Phosphorylated residues in the vicinity of the N-terminal FANCD2 degron detected in this and other studies.

I. Immunoblots showing levels of transiently transfected FANCD2-WT and K561R mutant in the absence or presence of an increasing amount of co-transfected FLAG-FBXL12.

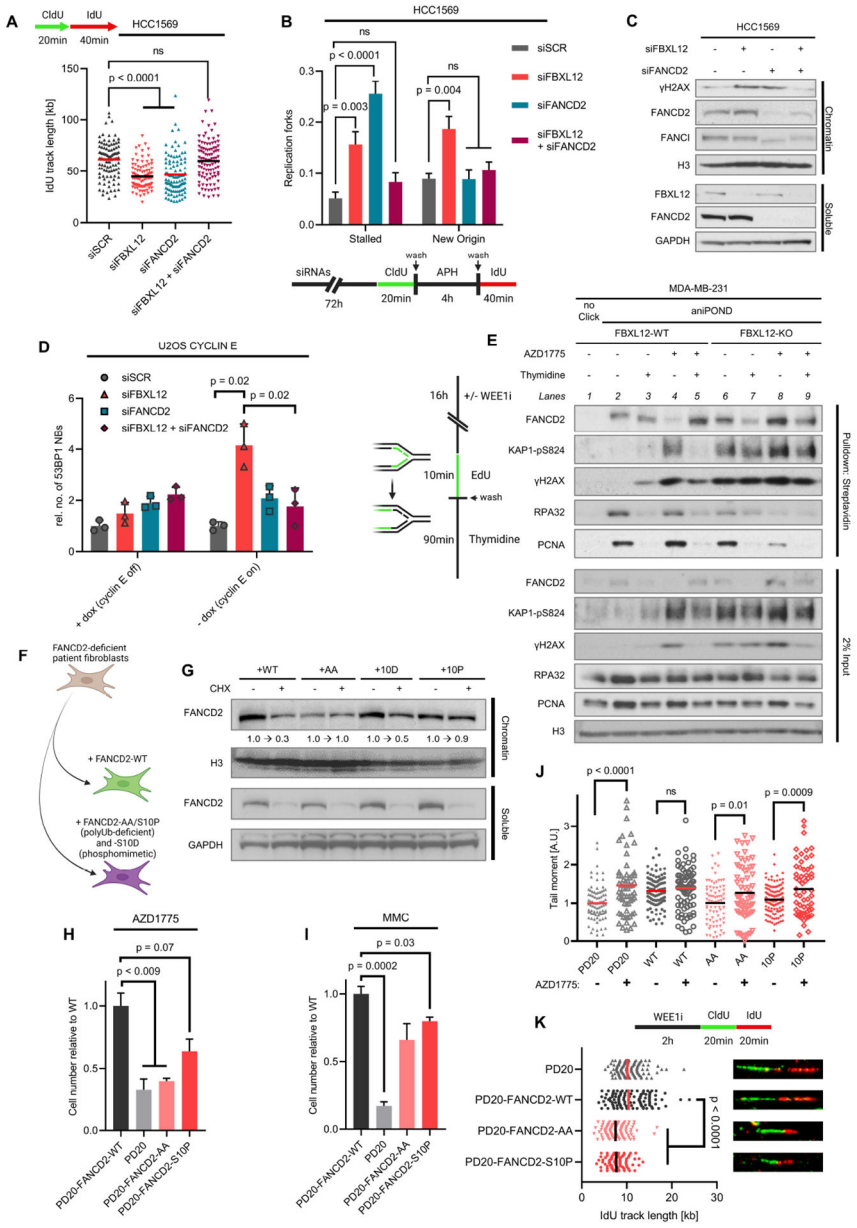

Fig. 6.

FBXL12 alleviates replication stress in a FANCD2-dependent manner

A. DNA fibre assay of HCC1569 cells transfected with control, FBXL12 or FANCD2 siRNAs, and labelled as indicated in the schematic. IdU track lengths plotted are from >100 fibres scored per condition.

B. HCC1569 were transfected as in panel A and replication recovery assessed. Presented data represent mean of three experiments and >200 replication tracks assessed.

C. Immunoblots of chromatin and soluble lysate fractions from HCC1569 cells transfected as in panel A.

D. 53BP1 nuclear bodies in cyclin A-negative G1 cells. U2OS CYCLIN E cells were transfected with the indicated siRNAs, cultured ± doxycycline for 24h, then subjected to HU

treatment for 24h followed by drug wash-out for another 24h. Presented data are the mean 53BP1 nuclear body numbers relative to control cells.

E. aniPOND analysis of proteins present at newly replicated DNA and at regions up to 90min after passing of the replication fork. Blots show the situation in FBXL12-WT or KO MDA-MB-231 cells treated as indicated in the schematic (left).

F. Reconstitution of PD20 FANCD2-deficient fibroblasts with WT, polyubiquitination-deficient and phosphomimetic FANCD2 mutants.

G. FANCD2 CHX chase in PD20 cells ± WT or mutant FANCD2. Cells were pre-treated with MMC for 4h followed by 4h MMC wash-out in the presence of CHX.

H. Quantification of PD20 colony formation assay after treatment with WEE1i AZD1775.

I. Quantification of PD20 colony formation assay after treatment with cross-linking agent MMC.

J. Comet assay performed under alkaline conditions indicating the presence of DNA damage under untreated conditions and upon 2h AZD1775 treatment in PD20 ± FANCD2-WT, AA or S10P mutants.

K. DNA fibre assay of PD20 ± FANCD2-WT, -AA or S10P mutant. Cells were pre-treated with 500nM WEE1i AZD1775 and pulse-labelled as indicated. IdU track lengths are plotted from >100 fibres measured per condition.

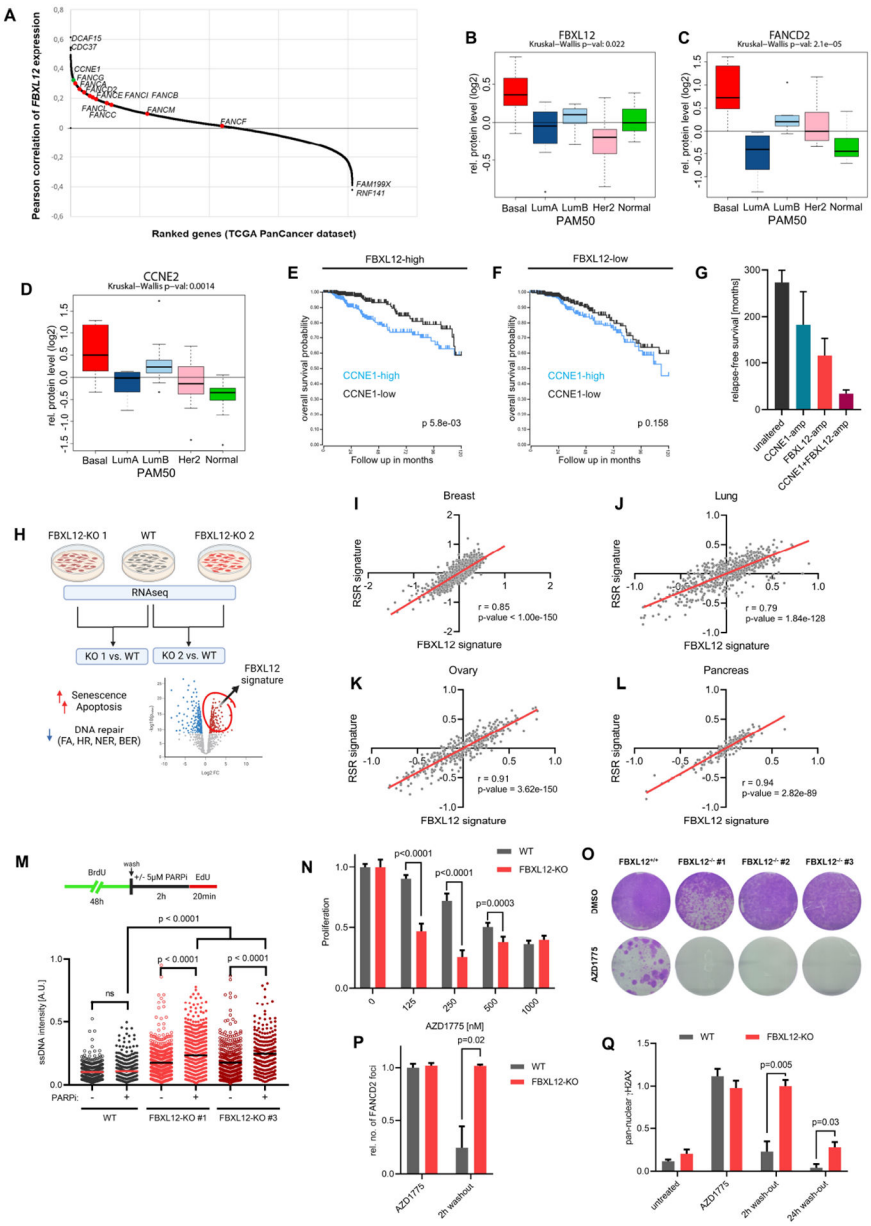

Fig. 7.

The FBXL12-FANCD2 axis is over-expressed in highly proliferative tumours and its disruption causes sensitisation to drug-induced replication stress

A. Pairwise correlation analysis of FBXL12 mRNA and 20311 mRNAs from 9066 samples in the TCGA PanCancer cohort[55]. Datapoints for CCNE1 mRNA and FA genes are indicated in green and red, respectively.

B. FBXL12 protein levels in 45 human breast cancers stratified based on PAM50 grouping. Y-axis indicates median normalised relative protein levels.

C. FANCD2 protein levels in breast cancers as in panel B.

D. CYCLIN E2 protein levels in breast cancers as in panel B.

E. Kaplan-Meier overall survival of the TCGA invasive breast carcinoma patient cohort[55] with above median FBXL12 mRNA expression levels. Blue and black curves denote groups with high and low *CCNE1* with a median expression cut-off.

F. Kaplan-Meier overall survival as in panel E but with below median FBXL12 mRNA expression levels.

G. Median survival of breast cancers patients from the METABRIC cohort subdivided based on the presence of *CCNE1* and *FBXL12* amplifications.

H. Scheme outlining the steps to identify an FBXL12-KO associated gene expression signature consisting of genes upregulated across two MDA-MB-231 FBXL12-KO clones.

I. Correlation between the FBXL12-KO signature and an RS response signature (from[56]) using TCGA gene expression datasets on an invasive breast carcinoma cohort.

J. Lung adenocarcinoma cohort analysed as in panel I.

K. Ovarian serous cystadenocarcinoma cohort analysed as in panel I.

L. Pancreatic adenocarcinoma cohort analysed as in panel I.

M. Analysis of replication-associated ssDNA generation upon PARPi (Olaparib) treatment. Schematic and quantification of ssDNA intensity of EdU-positive nuclei. Per condition a minimum of 250 nuclei were scored.

N. Proliferation of MDA-MB-231 FBXL12-WT and FBXL12-KO cell lines treated with increasing concentrations of WEE1 inhibitor AZD1775 for 72h.

O. Colony formation of MDA-MB-231 FBXL12-WT and FBXL12-KO cell lines treated with AZD1775 for 72h, and subsequently allowed to recover for 10 days.

P. FANCD2 foci numbers upon 4h AZD1775 treatment in MDA-MB-231 FBXL12-WT and FBXL12-KO cells assessed using HCI. Mean numbers of FANCD2 foci relative to untreated controls are plotted.

Q. Pan-nuclear γH2AX staining upon 4h AZD1775 treatment of MDA-MB-231 FBXL12-WT and FBXL12-KO cells assessed using HCI. Mean numbers relative to untreated controls are plotted.

KEY RESOURCES TABLE

REAGENT or RESOURCE	SOURCE	IDENTIFIER
Antibodies		
Rabbit polyclonal FBXL12	Atlas antibodies	2843
Goat polyclonal FBXL12	Novus Biologicals	1295
Rabbit polyclonal FANCD2	Cell Signaling Technology	16323
Mouse monoclonal FANCD2	Santa Cruz Biotechnology	sc-20022
Rabbit polyclonal FANCI	Cell Signaling Technology	14657
Mouse monoclonal CYCLIN E	Santa Cruz Biotechnology	sc-247
Mouse monoclonal γH2AX	Sigma-Aldrich	05–636
Rabbit monoclonal γH2AX	Cell Signaling Technology	9718
Rabbit polyclonal GAPDH	Santa Cruz Biotechnology	sc-25778
Mouse monoclonal PCNA	Santa Cruz Biotechnology	sc-25280
Mouse monoclonal H3	Cell Signaling Technology	3638
Rabbit polyclonal H3-pS10	Sigma-Aldrich	06–570
Mouse monoclonal MYC	Santa Cruz Biotechnology	sc-40
Mouse monoclonal HA	Sigma-Aldrich	H3663
Rabbit polyclonal HA	Sigma-Aldrich	H6908
Rabbit polyclonal FLAG	Sigma-Aldrich	F7425
Mouse monoclonal p21	Santa Cruz Biotechnology	sc-6246
Rabbit monoclonal RAD51	Cell Signaling Technology	8875
Rabbit monoclonal RAD51	Abcam	ab133534
Mouse monoclonal CHK1	Cell Signaling Technology	2360
Rabbit monoclonal CHK1-pS345	Cell Signaling Technology	2348
Rabbit polyclonal RPA32	GeneTex	GTX70258
Mouse monoclonal BrdU	Invitrogen	B35128
Rat monoclonal BrdU (to detect CldU)	Abcam	ab6326
Mouse monoclonal BrdU (to detect IdU)	BD Biosciences	347580
Mouse monoclonal PICH	Sigma-Aldrich	04–1540
Rabbit polyclonal GFP	Santa Cruz Biotechnology	sc-8334
Mouse monoclonal Ubiquitin	Sigma-Aldrich	MAB1510
Rabbit monoclonal RXXpS/pT	Cell Signaling Technology	9614 (110B7E)
Rabbit polyclonal KAP1-PS824	Cell Signaling Technology	4127
Bacterial and virus strains		
One Shot™ TOP10 *E.coli*	Thermo Fisher Scientific	C404003
One Shot™ Stbl3 *E.coli*	Thermo Fisher Scientific	C737303
Chemicals, peptides, and recombinant proteins		
WEE1 inhibitor AZD1775	Selleckchem	S1525
ATR inhibitor AZD6738	Selleckchem	S7693

REAGENT or RESOURCE	SOURCE	IDENTIFIER
CHK1/2 inhibitor AZD7762	Selleckchem	S1532
CHK1 inhibitor Rabusertib	Selleckchem	S2626
DNA-PK inhibitor NU7441	Selleckchem	S2638
CDC7 inhibitor XL413	Selleckchem	S7547
Aphidicolin	Sigma-Aldrich	A0781
Hydroxyurea	Sigma-Aldrich	400046
Mitomycin C	Sigma-Aldrich	M4287
Cisplatin	Sigma-Aldrich	232120
MLN4924	Selleckchem	S7109
MG-132	Selleckchem	S2619
Epoxomicin	Selleckchem	S7038
Bortezomib	Selleckchem	S1013
RO-3306	Selleckchem	S7747
EdU	Sigma-Aldrich	900584
BrdU	Thermo Fisher Scientific	B23151
CldU	Sigma-Aldrich	C6891
IdU	Sigma-Aldrich	I7125
Doxycyclin	Sigma-Aldrich	D3447
Puromycin	Sigma-Aldrich	P7255
Mammary epithelial growth supplement	Thermo Fisher Scientific	S0155
PhosSTOP™ phosphatase inhibitors	Sigma-Aldrich	4906845001
cOmplete™ protease inhibitors	Sigma-Aldrich	11836170001
NEM	Selleckchem	S3692
Hoechst33342	Thermo Fisher Scientific	62249
Polybrene	R&D systems	7711
LT-1	Mirus Bio	MIR2300
HiPerfect	Qiagen	301705
Biotin azide	Jena Bioscience	CLK-1265
X-Gal	Sigma-Aldrich	XGAL-RO
Crystal violet	Sigma-Aldrich	61135
Alamar blue	Sigma-Aldrich	R7017
SYBR™ Green	Thermo Fisher Scientific	S7563
ProLong Diamond mountant	Thermo Fisher Scientific	P36961
FANCD2 N-terminal peptide WT - MVSKRRLSKSEDKE	GenScript	n/a
FANCD2 N-terminal peptide S8/10A - MVSKRRLAKAEDKE	GenScript	n/a
Recombinant Ubiquitin	R&D systems	U-100H
Recombinant UBA1	MedChemExpress	HY-P74485
Recombinant UBCH3	R&D systems	E2–610
Recombinant CHK1	R&D systems	1630-KS

REAGENT or RESOURCE	SOURCE	IDENTIFIER
Recombinant GSK3β	R&D systems	2506-KS
Critical commercial assays		
EdU Click-iT™ kit 488	Thermo Fisher Scientific	C10420
EdU Click-iT™ kit 594	Thermo Fisher Scientific	C10646
RNeasy Plus mini kit	Qiagen	74134
RNA 6000 Nano kit	Agilent	5067–1511
Q5® site-directed mutagenesis kit	New England Biolabs	E0554S
TnT® Quick Coupled Transcription/Translation System	Promega	L1170
Deposited data		
Replication recovery screen data	This paper; Mendeley Data	doi: 10.17632/4nwt3dz3k6.1
MS FBXL12-IP data	This paper; MassIVE	MSV000092004
MS FANCD2-IP phosphoproteomics data	This paper; ProteomeXchange	PXD043637
MDA-MB-231 FBXL12-WT/KO RNAseq data	This paper; GEO	GSE232558
Experimental models: Cell lines		
HCC1569	ATCC	CRL-2330
HCC1569 shSCRAMBLED	this paper	n/a
HCC1569 shFBXL12	this paper	n/a
U2OS CYCLIN E tet-off	Jiří Bártek[1]	n/a
HEK293/293T	ATCC	CRL-3216
HEK293T FBXL12-KO	this paper	n/a
Flp-In T-REx-293 FBXL12	this paper	n/a
MCF10A	ATCC	CRL-10317
MCF10A shSCRAMBLED	this paper	n/a
MCF10A shFBXL12	this paper	n/a
RPE-1	ATCC	CRL-4000
MDA-MB-231	ATCC	CRM-HTB-26
MDA-MB-231 gSCRAMBLED	Brunner et al.[2]	n/a
MDA-MB-231 FBXL12-KO	this paper	n/a
MDA-MB-231 shSCRAMBLED	this paper	n/a
MDA-MB-231 shFBXL12	this paper	n/a
MDA-MB-157	ATCC	HTB-24
SUM149PT	BioIVT	HUMANSUM-0003004
Cal51	DSMZ	ACC302
HCC1419	ATCC	CRL-2326
MCF7	ATCC	HTB-22
HCT116	Bert Vogelstein[3]	n/a
HCT116 FBXW7-KO	Bert Vogelstein[3]	n/a
PD20	Fanconi anemia research fund[4,5]	n/a

REAGENT or RESOURCE	SOURCE	IDENTIFIER
PD20-FANCD2-WT	this paper	n/a
PD20-FANCD2-AA	this paper	n/a
PD20-FANCD2-S10P	this paper	n/a
PD20-FANCD2-S10D	this paper	n/a
Oligonucleotides		
Silencer Select Human DNA Damage Response siRNA Library	Thermo Fisher Scientific	A30089
siFBXL12 5'-UGAUCGAUAUGCUCAUAAA-3' and 5'-GCGAUUCAAUGAUCGAU-3'	Qiagen	SI00119266 and SI00119287
ON-TARGETplus SMARTPool siFANCD2	Dharmacon	L-016376–00
ON-TARGETplus SMARTPool siFANCI	Dharmacon	L-022320–01
siUSP1	Qiagen	SI03155439
siFANCL 5'-GACAAGAGCTGTATGCACT-3'	Meetei et al., 2003[6]	n/a
siSCRAMBLED 5'-AGGUAGUGUAAUCGCCUUG-3'	Eurofins Genomics	n/a
PrimeTime™ qPCR primer FBXL12 5'-TGCTCGAGATCTTCTCTTACCT-3' and 5'-GACTTTAGGTCGCATCGTGTA-3'	IDT	Hs.PT.58.1255276
PrimeTime™ qPCR primer CCNE1 5'-CAACATACAGACCCACAGAGAC-3' and 5'-GAGAAGCCCTATTTTGTTCAGAC-3'	IDT	Hs.PT.56a.27776605
PrimeTime™ qPCR primer FANCD2 5'-CTCCACATTCCCTACACTGAC-3' and 5'-CATGAATCTGCTGCGAGTCT-3'	IDT	Hs.PT.58.3347498
qPCR primer GAPDH 5'-ACATCGCTCAGACACCATG-3' and 5'-TGTAGTTGAGGTCAATGAAGGG-3'	IDT	Hs.PT.39a.22214836
Recombinant DNA		
pTRIPZ	Dharmacon	n/a
pTRIPZ-shSCRAMBLED	this paper	n/a
pTRIPZ-shFBXL12	this paper	n/a
pTRIPZ-FLAG-FBXL12	this paper	n/a
pTRIPZ-FLAG-FBXL12-ΔF	this paper	n/a
pX462	Feng Zhang[7]	Addgene #48141
pLenti-CRISPR V2	Feng Zhang[8]	Addgene #52961
psPAX2	Didier Trono	Addgene #12260
pMD2.G	Didier Trono	Addgene #12259
pCMV2	Sigma-Aldrich	E7033
pCMV2-FLAG-FBXL12	this paper	n/a
pEGFP-N2-FBXL12-ΔF	this paper	n/a
pEGFP-N2	Clontech	6081–1
pEGFP-N2-FBXL12	this paper	n/a
pcDNA3.1-MYC-FANCD2	this paper	n/a
pcDNA3.1-MYC-FANCD2-AA	this paper	n/a
pcDNA3.1-MYC-FANCD2-K561R	this paper	n/a
pcDNA3.1-MYC-FANCD2–2KR	this paper	n/a

REAGENT or RESOURCE	SOURCE	IDENTIFIER
pcDNA3.1-MYC-FANCD2–7KR	this paper	n/a
pcDNA3.1-HA-FANCD2	this paper	n/a
pcDNA3.1-HA-FANCD2-AA	this paper	n/a
pLV-FANCD2	Vectorbuilder	VB900001–6862vjs
pLV-FANCD2-AA	this paper	n/a
pLV-FANCD2-S10P	this paper	n/a
pLV-FANCD2-S10D	this paper	n/a
pDEST-CMV-FLAG-FANCI	Tony Huang[9]	n/a
pcDNA3.1-HA-CUL1	Yue Xiong[10]	n/a
pcDNA3.1-HA-dnCUL1	Yue Xiong[10]	n/a
HA-Ubiquitin	Edward Yeh[11]	Addgene #18712
GFP-Ubiquitin	Nico Dantuma[12]	Addgene #11928
Software and algorithms		
CellProfiler	https://cellprofiler.org/ [13]	n/a
GraphPad Prism 9	Graphpad	n/a
BioRender	BioRender.com	n/a
Galaxy Europe	https://usegalaxy.eu/	n/a
R	https://cran.r-project.org [14]	n/a
ImageJ	https://imagej.net/Download	n/a
Proteome Discoverer	Thermo Fisher Scientific	n/a
OpenComet	https://cometbio.org/	n/a
Other		
Dynabeads™ Protein G	Thermo Fisher Scientific	10004D
Dynabeads™ MyOne™ Streptavidin T1	Thermo Fisher Scientific	65604
TUBE 2 magnetic beads	LifeSensors	UM402M